AFBMD-TR-59-21

Air Force Ballistic Missile Division
Air Research and Development Command
United States Air Force
Inglewood, California
Contract No. AF 04(647)-176

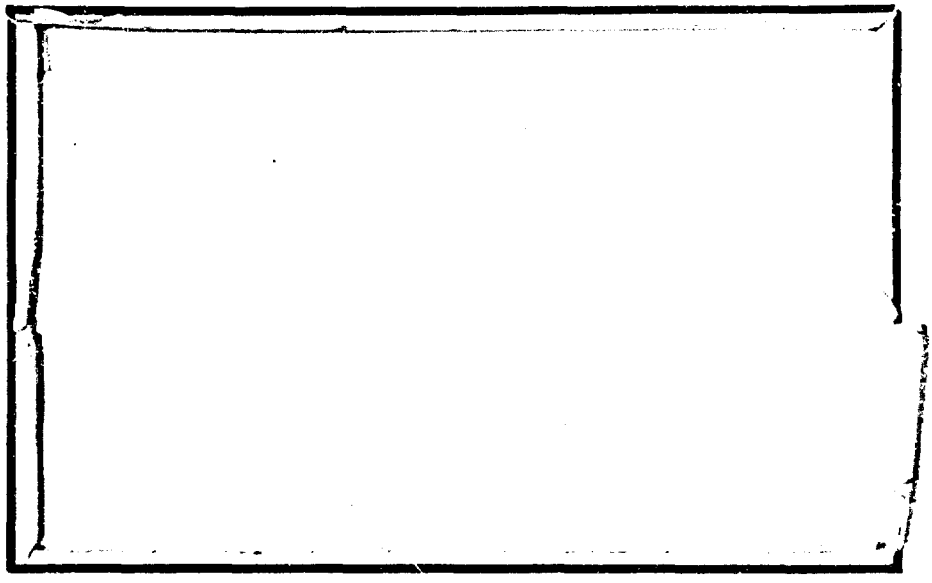

DEPARTMENT OF ELECTRICAL ENGINEERING

UNIVERSITY OF UTAH

SALT LAKE CITY, UTAH

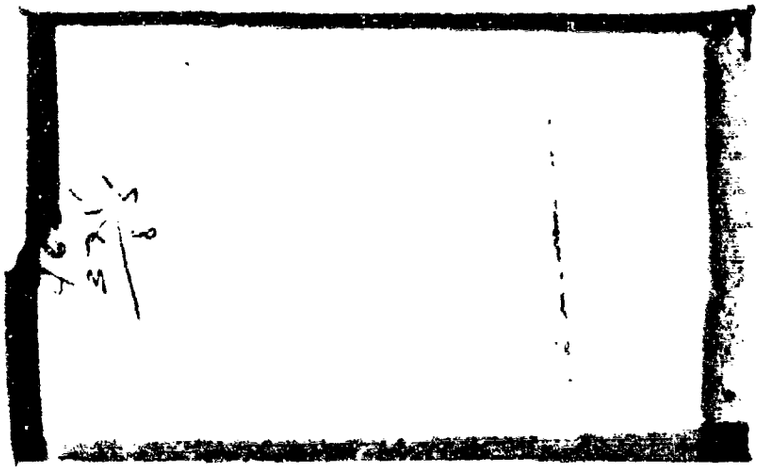

Department of Electrical Engineering, University of Utah, Salt Lake City, Utah.
CRATERING PRODUCED IN METALS BY HIGH-VELOCITY IMPACT, by D. K. Johnson, E. T. Cannon, E. P. Palmer, and R. W. Grow. Technical Report UU-4, July 31, 1959, 69 p., figures, tables. Penetration and cratering study, Air Force Ballistic Missiles Division, Contract No. AF 04(647)-176.

Steel spheres were accelerated to velocities up to 2.9 km/sec and impacted on targets of copper, lead, aluminum, magnesium, zinc, silver, and 4130 steel. Volume, area, and depth of the resulting craters are plotted as functions of projectile energy or momentum. Crater volume was found to be proportional to projectile energy. Relationships between volume per unit energy and compressive yield strength and shear strength of the targets were found. Area and penetration were dependent on projectile deformation as well as velocity.

University of Utah
Johnson, D. K., Cannon, E. T., Palmer, E. P., Grow, R. W.
Contract No. AF 04(647)-176, Air Force Ballistic Missile Division

Cratering
High-velocity Impact

Penetration and Cratering Study
Air Force Ballistic Missiles Division
Contract No. AF 04(647)-176

CRATERING PRODUCED IN METALS BY HIGH-VELOCITY IMPACT

D. K. Johnson, E. T. Cannon,
E. P. Palmer, and R. W. Grow

Technical Report UU-4

July 31, 1959

ACKNOWLEDGMENTS

The authors wish to express their appreciation to the Air Force Ballistic Missile Division (ARDC) who sponsored the research presented in this report and to the Space Technology Laboratories in providing technical direction for the Air Force. Appreciation is also extended to Donald L. Greenhalgh for his aid in gathering the experimental data, and to Gerald E. Peterson for his diligent efforts in preparing the photographs.

ABSTRACT

Steel spheres having a diameter of 3/16 inch (0.476 cm) were accelerated with a 220 caliber or a 243 caliber smooth-bore gun up to velocities of 2.5 kilometers per second. The spheres were impacted normally upon targets of copper, lead, aluminum, magnesium, zinc, silver, and 4140 steel. The area, volume, and depth of the resulting craters were measured and plotted as a function of either the initial impact energy or the initial impact momentum of the projectile.

The crater volume was found to be a linear function of the projectile energy for all targets. A relationship was found to exist between the volume per unit energy and the static compressive yield strength and static shear strength of the various target materials. A plot of crater area versus projectile momentum was found to have two linear segments.

The penetration, or maximum depth of the crater, was plotted as a function of the projectile momentum. A region of negative slope for penetration versus momentum was found for the aluminum, lead, and magnesium targets. The other targets did not have this region.

Partridge, VanFleet, and Whited[1,2] presented data for many of the same targets impacted with spheres of the same material as the target. Comparisons were made between their data and the data obtained using steel spheres for the projectile. Correlation between the data was excellent in most cases.

CONTENTS

INTRODUCTION

With the development of missiles and satellites, interest has developed in the phenomena associated with objects moving with high velocities. Satellite velocities range up to 11.2 km/sec, and meteoric particles, in the vicinity of the earth, have velocities extending to 73 kilometers per second.[3] With the possibility of collisions between space vehicles and particles having these velocities, it is desirable to know the effects the particles produce on the impacted surfaces. This report is concerned with the impact phenomena associated with high velocity objects.

In an attempt to better understand the properties of materials under impact loads, projectiles were accelerated and impacted into targets of different materials. The materials used for targets were: lead, copper, aluminum, magnesium, zinc, 4140 steel, and silver. Targets were selected so there would be a variety of characteristics to compare. Spheres were used for the projectiles to eliminate the orientation variable. If cylinders were used for the projectiles, there would be some question as to which surface of the cylinder initially struck the target. In the experiments described in this report, steel spheres were used. By impacting all the previously mentioned targets with the same type projectile, it was hoped there would be some observable correlation between the known target material properties and the experimentally observed impact effects. Once the effects are known, the impact mechanisms can be deduced, and the principles applied to practical engineering design.

When a sphere is impacted against a target, a concentrated load of large magnitude is applied to the target. As a result, the surface of the target is deformed. This deformation is termed cratering. These craters were studied, and the results were presented in this report.

Previous research has been conducted into cratering phenomena.[1,2,4,5,6,7] Partridge, VanFleet, and Whited[1] did work similar to that presented in this paper. Many of the metals which they used for targets were also used in this investigation. The difference was in the projectile material; in all cases, their projectile material was the same as the target material. Data from their report will be quoted and compared with the data obtained using steel as the projectile.

EXPERIMENTAL PROCEDURE AND APPARATUS

High-Velocity Laboratory

This research into the effects of impact was done at the High-Velocity Laboratory, University of Utah. The laboratory is equipped with three concrete safety tunnels where explosives may be detonated. Firings in the tunnels are controlled from a position exterior to the tunnels.

Projectile (Particle) Acceleration

The projectiles used in this research were accelerated with explosives in a specially designed smooth bore gun. This gun consisted of two sections which were identical except for the ends. One section was designed so a breech could be attached, and the other section was designed for a vacuum adapter. The two sections, bolted together, formed the complete gun. A picture of a gun is shown in Fig. 1. During the course of the experiments, two calibers of guns were used. Initially, a 220 caliber was used, and later a 243 caliber gun was employed to raise the upper limit of velocity. Using explosives in these guns, the upper limit of velocity was about 2.5 kilometers per second. Firing was accomplished by means of a firing pin driven by a solenoid. The solenoid was electronically controlled from a console exterior to the tunnels. The solenoid and associated apparatus are shown in the right side of the picture in Fig. 1, and a picture of the console is shown in Fig. 2.

The apparatus on the front end of the gun in Fig. 1 is a vacuum

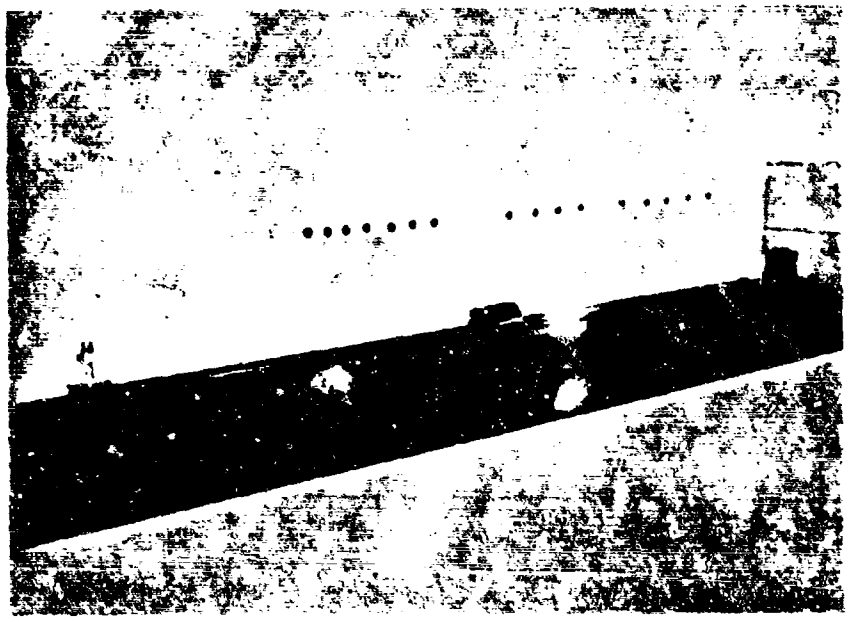

Fig. 1. - Gun for accelerating projectiles.

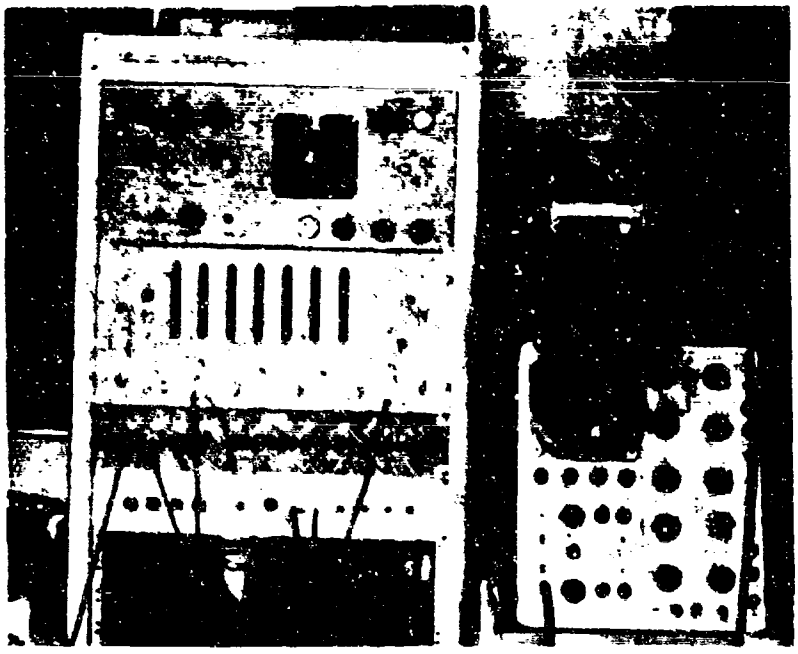

Fig. 2. - Console with Berkeley counter.

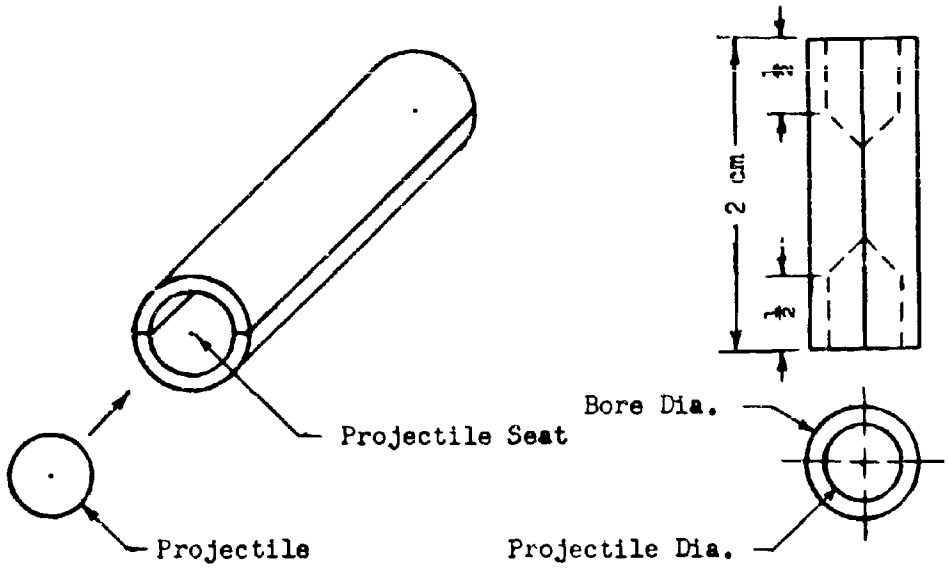

Fig. 3. - Sabot Dimensions.

adapter. This adapter made it possible to evacuate the barrel of the gun so slightly higher velocities could be obtained.

Sabots

All spheres fired in these experiments were enclosed in sabots while in the gun barrel. This was done to prevent contact between the sphere and the barrel, and thus prevent loss of the projectile's mass by friction against the barrel. A drawing of a typical sabot is shown in Fig. 3. The sabots were cylindrical and were bisected by a plane containing the axis of the cylinder. The bisection aided separation of the sabot and projectile as they emerged from the gun. Both ends of the sabot were drilled out; the front was drilled to seat the spherical projectile, and the rear drilled to facilitate the separation of the bisected sabot. The approximate dimensions of a sabot are shown in

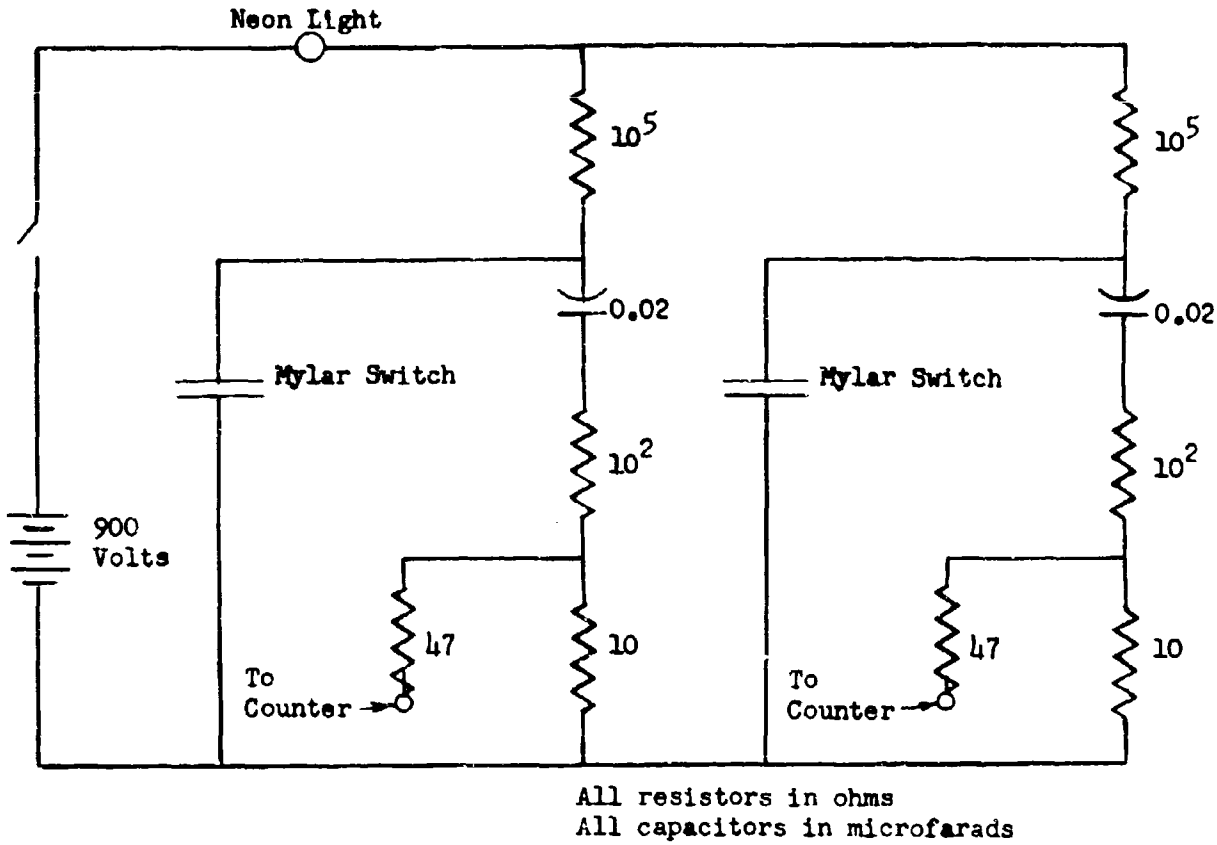

Fig. 4. - Schematic diagram of spider and mylar switches.

Fig. 3. The cylindrical sabots had an outside diameter equal to that of the gun bore and the length of about two centimeters. The sabots were made from a paper-reinforced, phenolic plastic.

A blast shield was placed immediately in front of the gun. The shield consisted of a steel plate with a central hole $\frac{1}{2}$ inch in diameter. After the sabot and projectile left the gun, the sabot separated from the projectile and hit the blast shield; the projectile then passed through the hole in the shield and proceeded alone toward the target.

Velocity-Measuring System

The system for measuring the projectile's velocity was placed between the blast shield and the target. This system consisted of a Berkeley

counter, to record elapsed time, an apparatus to control the counter, and aluminum-coated, mylar-plastic sheets.[8] The aluminum-coated, mylar sheets acted as switches and were placed in the path of the projectile. A potential was applied across the mylar insulator. When the aluminum-coated, mylar sheet was perforated by a projectile, the insulating mylar was broken, and the switch closed. This caused a capacitor to discharge through a resistor. The pulse across the resistor either started or stopped the Berkeley counter. When the projectile perforated the first mylar switch, the counter was started; when the second mylar switch was perforated, the counter was stopped. Thus, knowing the time between perforations and the distance between the mylar switches, the average velocity could be calculated. The capacitor, resistor control apparatus was called a "spider"; a circuit diagram of it is shown in Fig. 4.

A schematic drawing showing the arrangement of the "spider", gun, blast shield, mylar switches, and target is shown in Fig. 5.

Projectile Characteristics

The spherical projectiles used were commercial ball bearings[9] having a diameter of 3/16 inch (0.476 cm) and a mass of 440 milligram. The balls were manufactured from a high-carbon, chrome alloy steel thru-hardened to a hardness of 64-66 on the Rockwell C-scale. Throughout this report, these balls will be referred to as RC-66 steel. A number of RC-66 steel balls were annealed at 1200 ^{o}F and used as projectiles. The annealed balls were impacted into copper and aluminum targets only.

Crater Parameters

In this study three parameters are defined to describe the craters. They are crater volume, crater area, and crater depth or penetration.

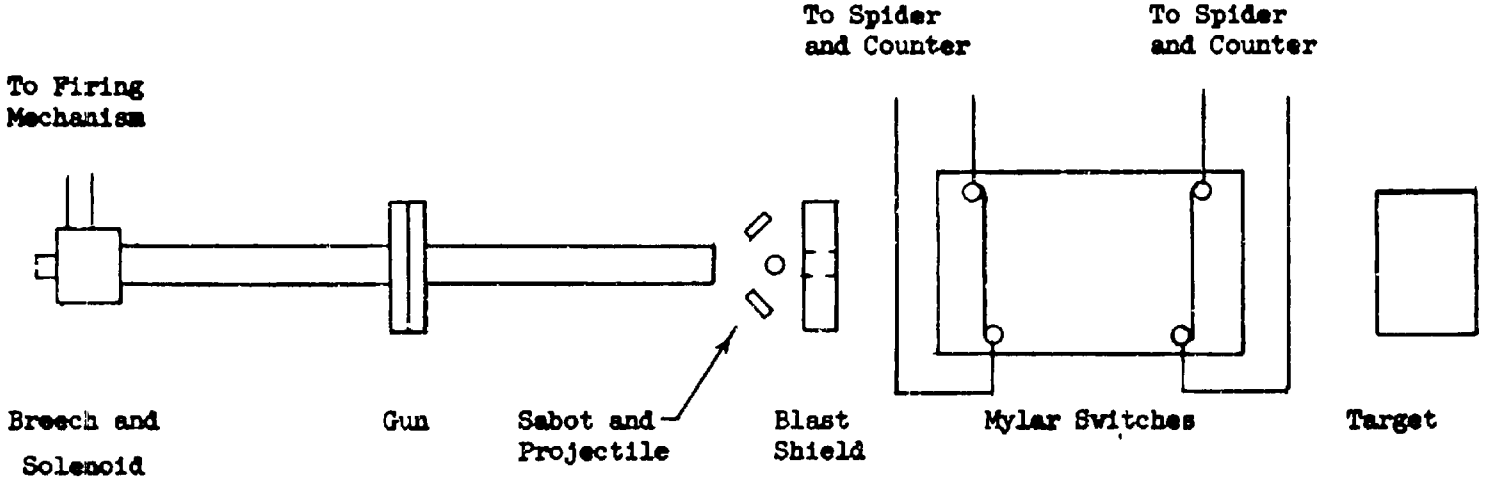

Fig. 5. - Top view of experimental apparatus showing the relative position of the various components.

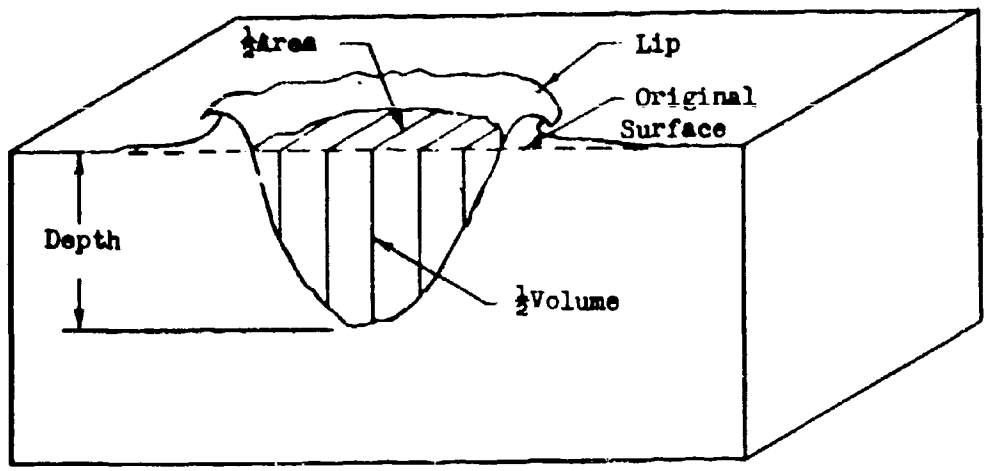

Fig. 6. - Cross section of typical crater.

A cross section of a typical crater is shown in Fig. 6 with the crater parameters indicated. Every crater has a lip as shown in Fig. 6. Before any measurements were made, this lip was removed to the level of the original target surface.

Crater volume is defined as the total volume of target material displaced. The volume of the crater was measured by filling it with a liquid from an automatic filling burette. An earlier method of measuring the volume consisted of filling the crater with melted wax. When the wax solidified, it was shaved to the surface of the target, removed from the crater, and weighed. Knowing the density of the wax, the volume of the wax inlay and the crater could be calculated. The tedious wax method was abandoned since the burette gave consistent results. The consistency of the burette method was within 2 to 3 per cent.

When the steel spheres were impacted into one of the aforementioned target materials, one of the following three things happened

to the projectile: (1) it bounced out of the crater, (2) it remained intact in the crater with nearly its original spherical shape, (3) it lost its spherical shape and fractured into distinct particles or became noticeably deformed. The RC-66 steel spheres fractured into distinct particles, and the annealed steel spheres simply deformed. The recorded data for crater volume, in the appendix, are with no steel projectile in the crater. If the steel sphere bounced out of the crater, there was no problem in measuring the volume. If the steel sphere remained intact in the crater, the entire sphere was assumed to be in the crater, and the sphere's volume was added to the measured crater volume. If the steel projectile fractured or deformed and adhered to the crater, it was removed before any volume measurement was made. The removal of the steel projectile was accomplished by immersing the target in an acid that would react with the steel and not the target. This acid technique could not be used on the 4140 steel targets, and it was impossible to distinguish with the naked eye between target steel and projectile steel. Hence, the recorded volume for craters in the 4140 steel targets is with the steel projectile in the crater.

Crater area is defined as the area of the crater at the original surface of the target. In calculating the crater area, it was assumed that a crater's cross section was circular. A number of diameter measurements were made with a cathotometer to determine an average diameter.

The penetration parameter is defined as the distance from the original target surface to the deepest point of the crater. The deepest point may or may not be in the center of the crater. This measurement was made with a spherometer in most cases. In aluminum

and magnesium, the craters were too narrow for the spherometer, and these two metals had to be cross sectioned. After cross sectioning, the depth of penetration was measured with the cathotometer.

EXPERIMENTAL RESULTS

The experimental results consist of qualitative observations and quantitative crater-parameter measurements. The parameters were plotted as either a function of the initial impact energy or a function of the initial impact momentum of t e projectile. Crater volume was plotted as a function of the energy while crater area was plotted as a function of the momentum. Figures 7 thru 15 are photographs of cross-sectioned craters impacted with RC-66 steel and annealed steel. These photographs will be utilized in discussing the qualitative results, and a familiarity with them adds to the understanding of the report. The steel projectiles and crater lips have been removed from the craters in the photographs. The velocity of the impacting projectile is shown below each crater.

From an inspection of the photographs of the cross-sectioned craters, the approximate velocity at which the steel projectile fractures or deforms can be determined. The cross section of the crater becomes noticeably broader after the fracture velocity is reached. In Fig. 7 the velocity at which the RC-66 steel fractures in zinc can be seen to lie between 0.79 and 1.00 km/sec. Similarly in Fig. 12, the fracture velocity of the RC-66 steel in magnesium can be observed to lie between 2.27 and 2.38 km/sec. The approximate fracture velocity for the other targets can also be determined from the cross-sectioned craters shown in the photographs. Another phenomenom is observed in aluminum, lead, and magnesium at the velocity at which the steel projectile fractures or deforms. The depth of penetration starts to decrease at this velocity in these metals. This fact can be observed for these metals in the photographs

of the cross-sectioned craters (Figs. 8, 9, 12, and 13).

Crater Volume

When crater volume is plotted as a function of the projectile energy, a linear relationship is found to exist. Figures 16 thru 22 are plots of volume versus energy for RC-66 steel projectiles. Figures 23 and 24 are volume versus energy relationships for annealed steel impacted into copper and aluminum. The slope of the volume versus energy line was calculated by the method of least squares. The results are shown in Table 1. Partridge, VanFleet, and Whited[1] also observed a linear relationship between volume and energy. Their results are shown for comparison in Table 1. It should be remembered that the target and projectile were of the same material for their experiments.

With the exception of aluminum, each target material in Table 1 shows about the same volume per unit energy regardless of the projectile. Partridge, VanFleet, and Whited[1] gave the value for volume per unit energy for aluminum without including any data or graph for volume versus energy. This omission makes one question that source of volume per unit energy value for aluminum. Discounting the aluminum data from this source, it appears that the volume per unit energy is essentially constant for a given target material. That is, the volume of target material displaced is independent of the projectile material. The displaced volume in a given target depends only upon the projectile's energy.

The shape of a crater in a given material is not independent of the projectile material. This fact can be seen by observing the cross section of aluminum and copper craters impacted with RC-66 steel and annealed steel (see Figs. 8, 9, 10, and 11). The RC-66 steel projectiles produce

Table 1. - Volume per unit energy for RC-66 steel projectiles, annealed steel projectiles, and corresponding data by Partridge, VanFleet, and Whited.[1]

Target Material	RC-66 Steel Projectiles	Annealed Steel Projectiles	Partridge, VanFleet and Whited Data[1]
Lead	4.25×10^{-9} m^3/joule		4.800×10^{-9} m^3/joule
Aluminum	1.67×10^{-9}	1.55×10^{-9} m^3/joule	0.776×10^{-9}
Silver	0.86×10^{-9}		0.800×10^{-9}
Magnesium	0.84×10^{-9}		
Zinc	0.65×10^{-9}		0.596×10^{-9}
Copper	0.60×10^{-9}	0.52×10^{-9}	0.588×10^{-9}
4140 Steel	0.20×10^{-9}		0.282×10^{-9} (Iron)

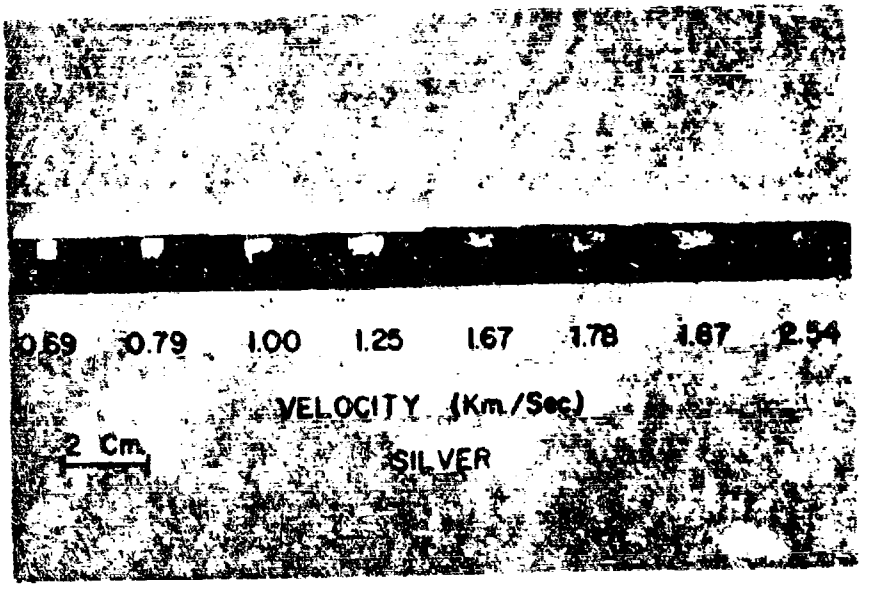

Fig. 7. - Cross-sectioned silver craters impacted with RC-66 steel.

narrower craters than those produced by the annealed steel. Although the shape of the craters in a material is different for different projectiles, the displaced volume at a specific projectile energy does not change appreciably.

Even with the same projectile material, the general shape of the crater changes with velocity. At velocities below which the RC-66 steel projectiles fracture, the crater is deep and narrow. This is especially noticeable in aluminum as shown in Fig. 8. When the projectile fractures, the general shape of the crater changes. The approximate velocity at which fracture occurs can be determined from the photographs of the cross-sectioned craters. At the fracture point, the cross section is wider than before fracture. Even though the shape of the crater changes with velocity, the volume per unit energy does not change at the fracture velocity. Each target material absorbs the projectile's energy in a manner that is independent of other actions of the projectile.

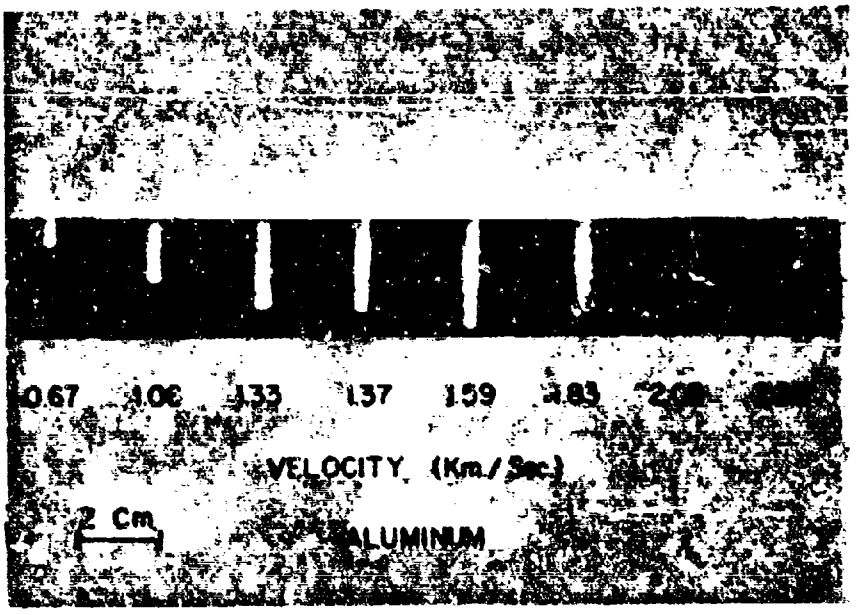

Fig. 8. - Cross-sectioned aluminum craters impacted with RC-66 steel.

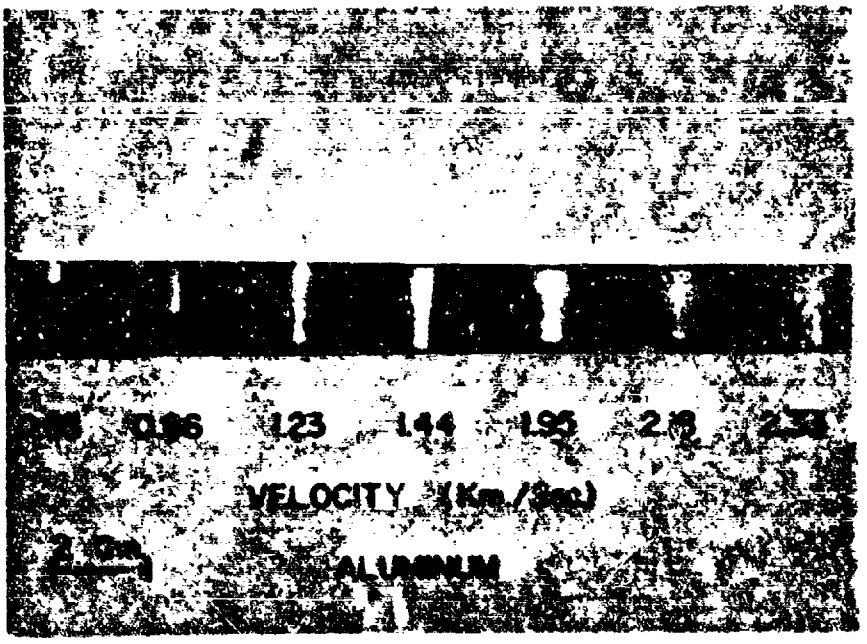

Fig. 9. - Cross-sectioned aluminum craters impacted with annealed steel.

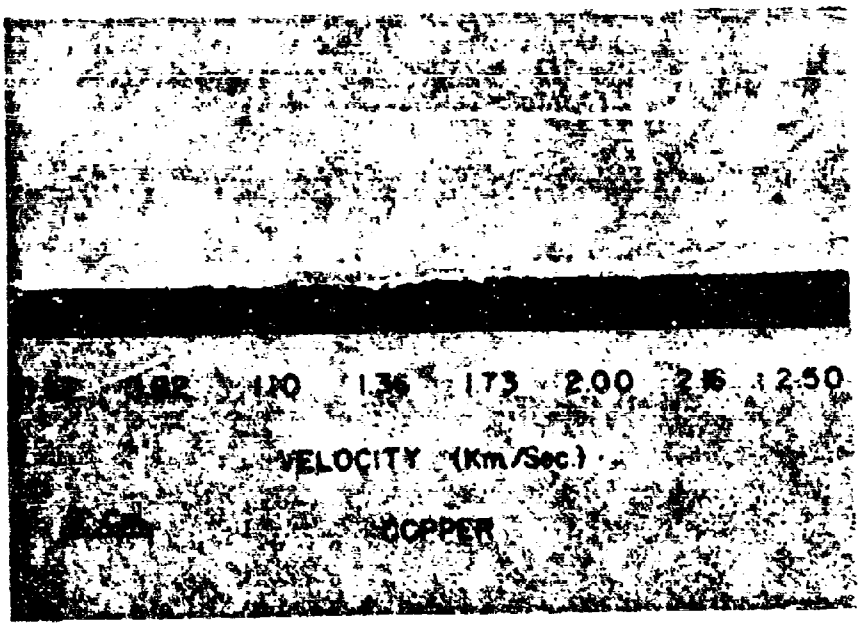

Fig. 10. - Cross-sectioned copper craters impacted with RC-66 steel.

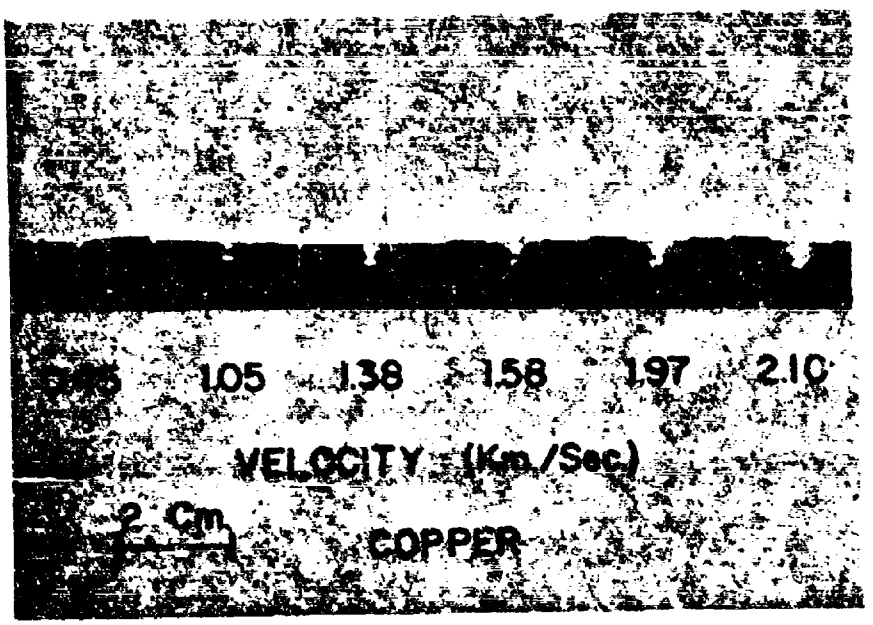

Fig. 11. - Cross-sectioned copper crater impacted with annealed steel.

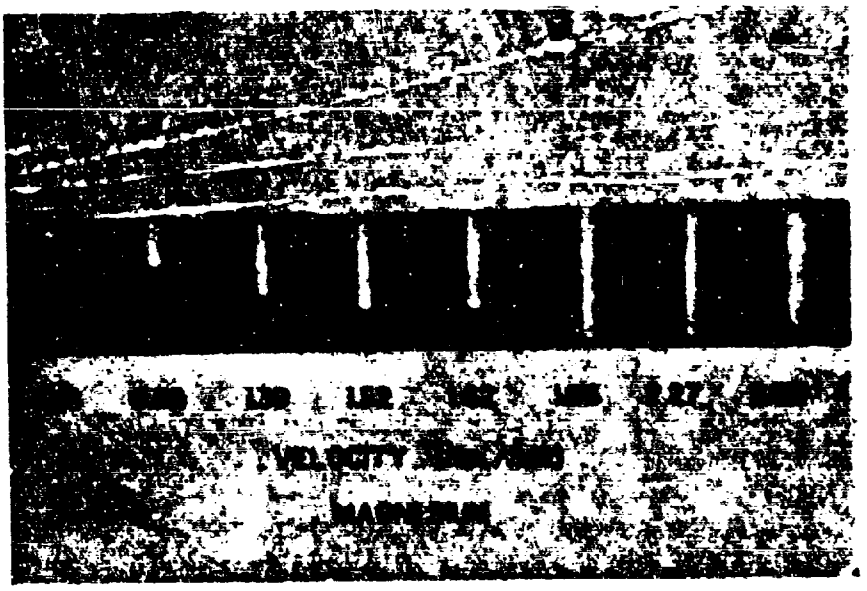

Fig. 12. - Cross-sectioned magnesium craters impacted with RC-66 steel.

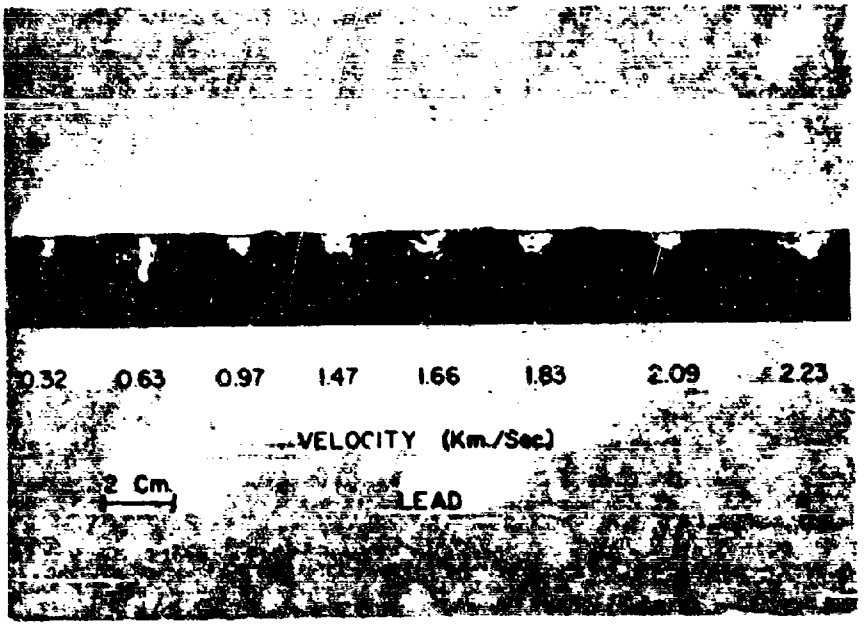

Fig. 13. - Cross-sectioned lead craters impacted with RC-66 steel.

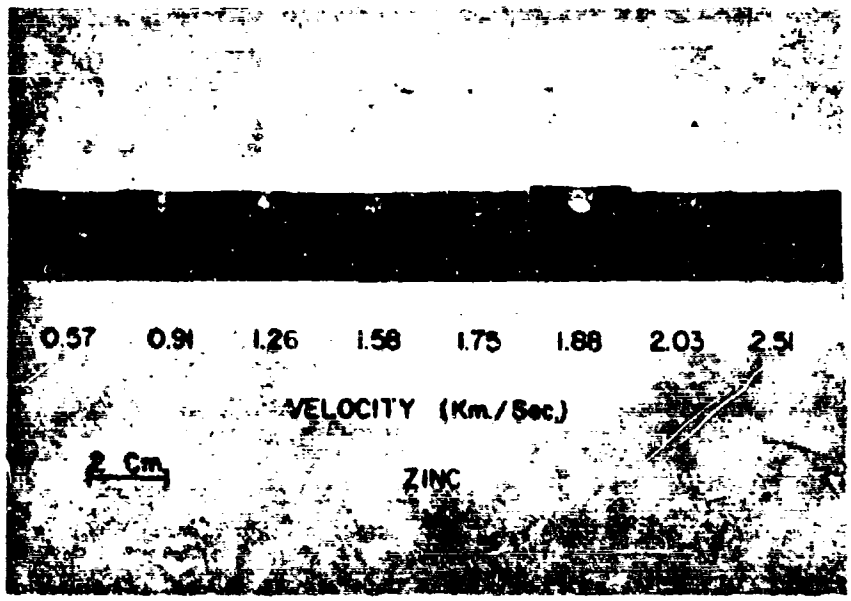

Fig. 14. - Cross-sectioned zinc craters impacted with RC-66 steel.

Fig. 15. - Cross-sectioned 4140 steel craters impacted with RC-66 steel.

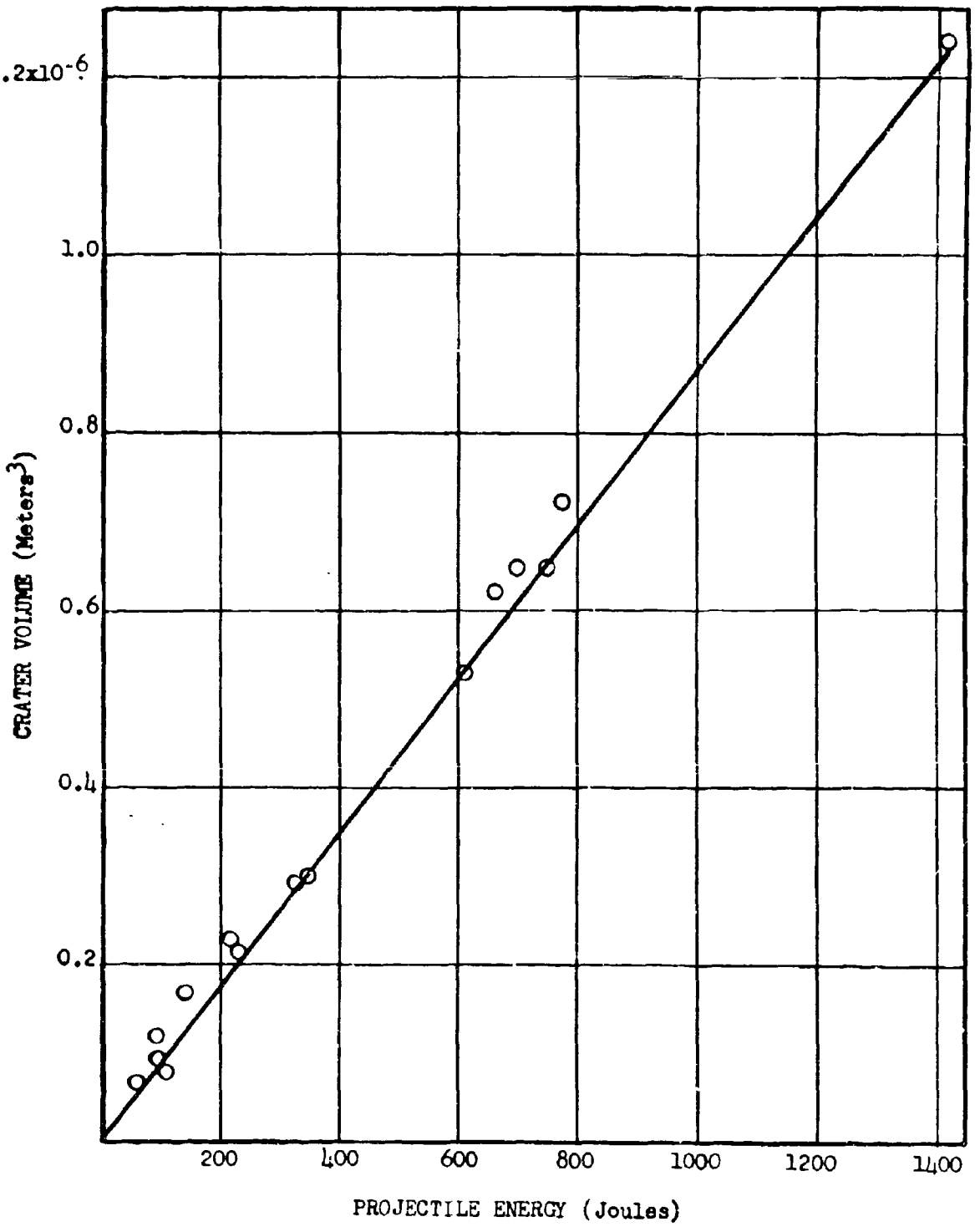

Fig. 16. - Crater volume versus projectile energy for RC-66 steel impacted into silver.

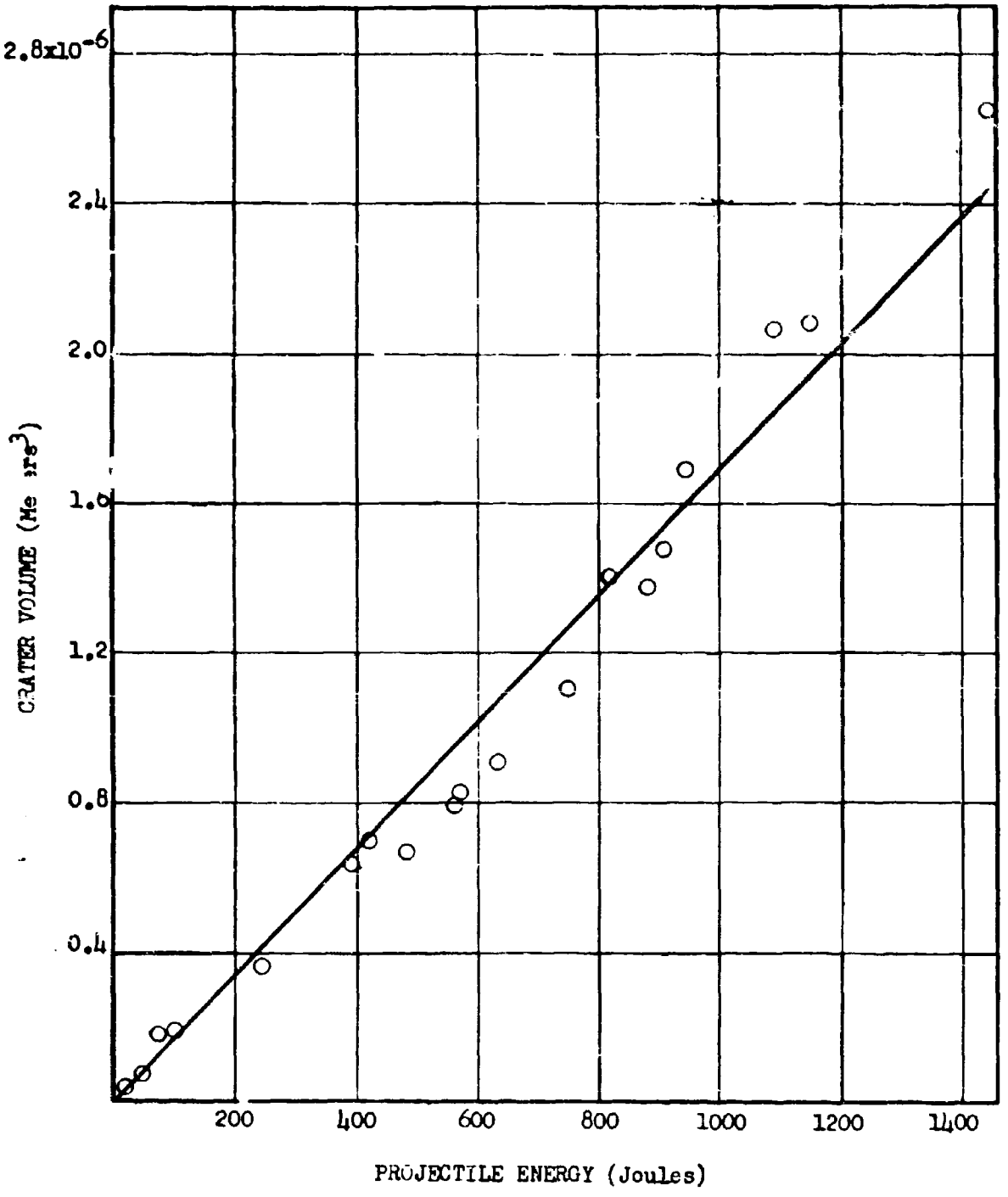

Fig. 17. - Crater Volume versus projectile energy for RC-66 steel impacted into aluminum.

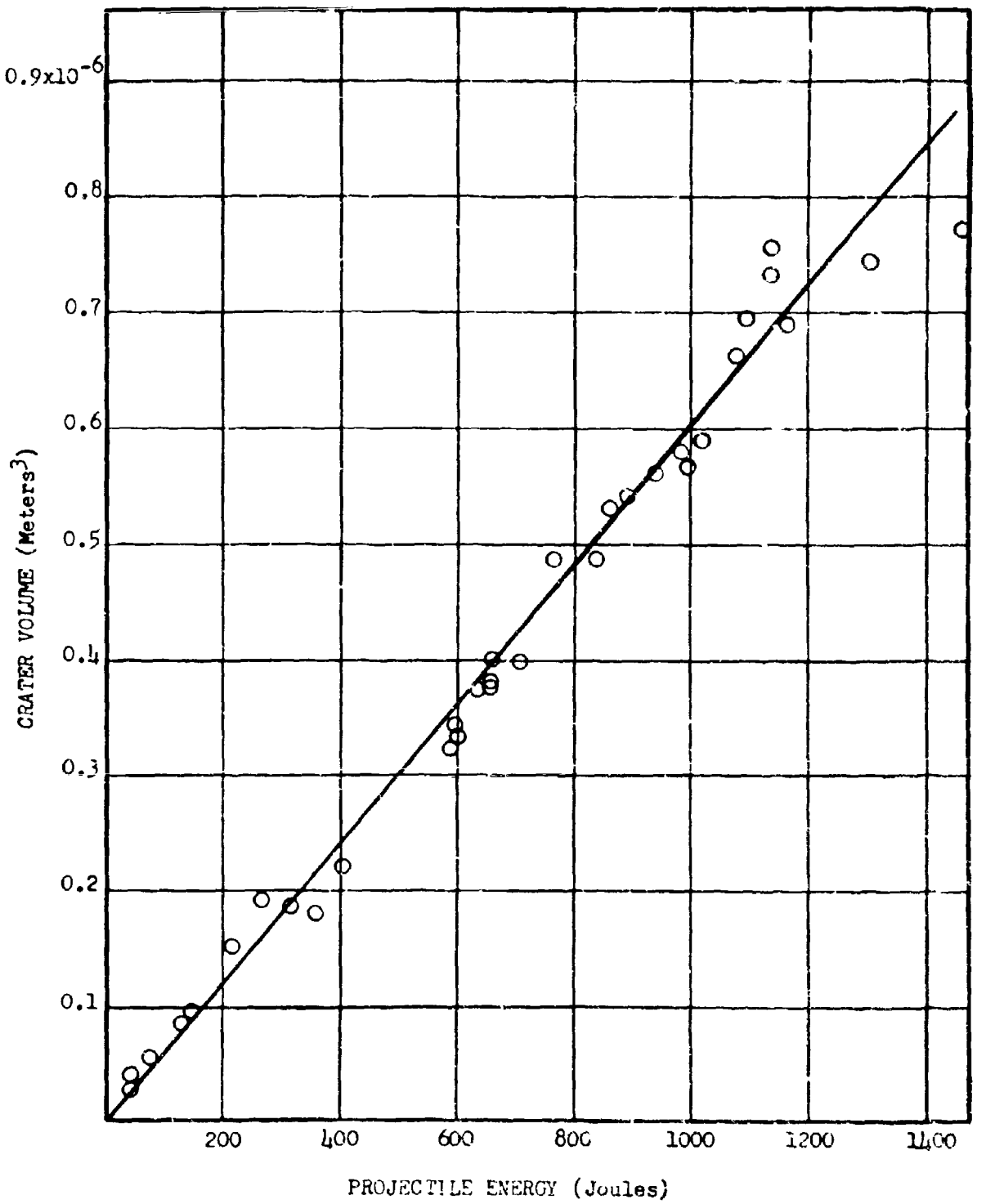

Fig. 18. - Crater volume versus projectile energy for RC-66 steel impacted into copper.

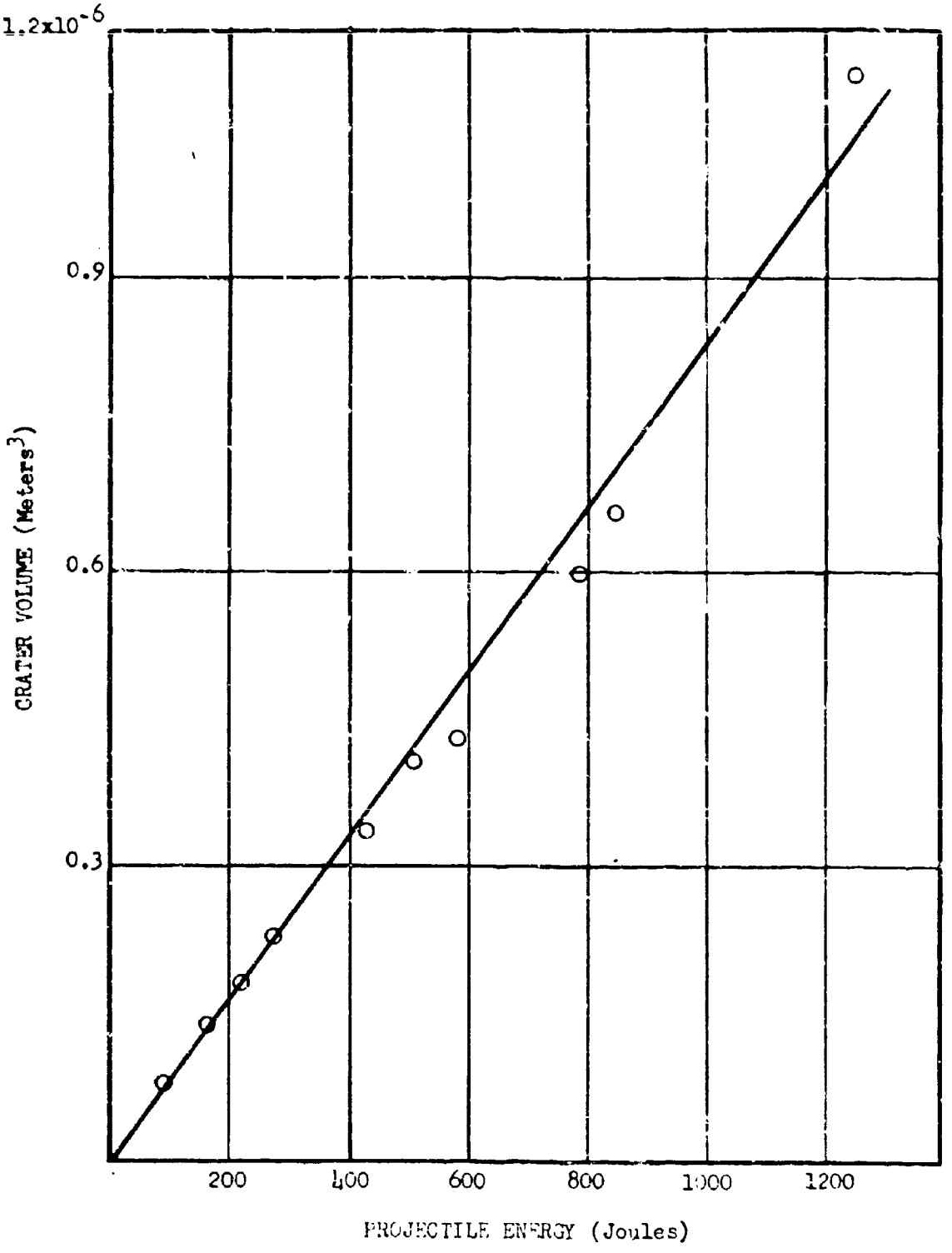

Fig. 19. - Crater volume versus projectile energy for RC-66 steel impacted into magnesium.

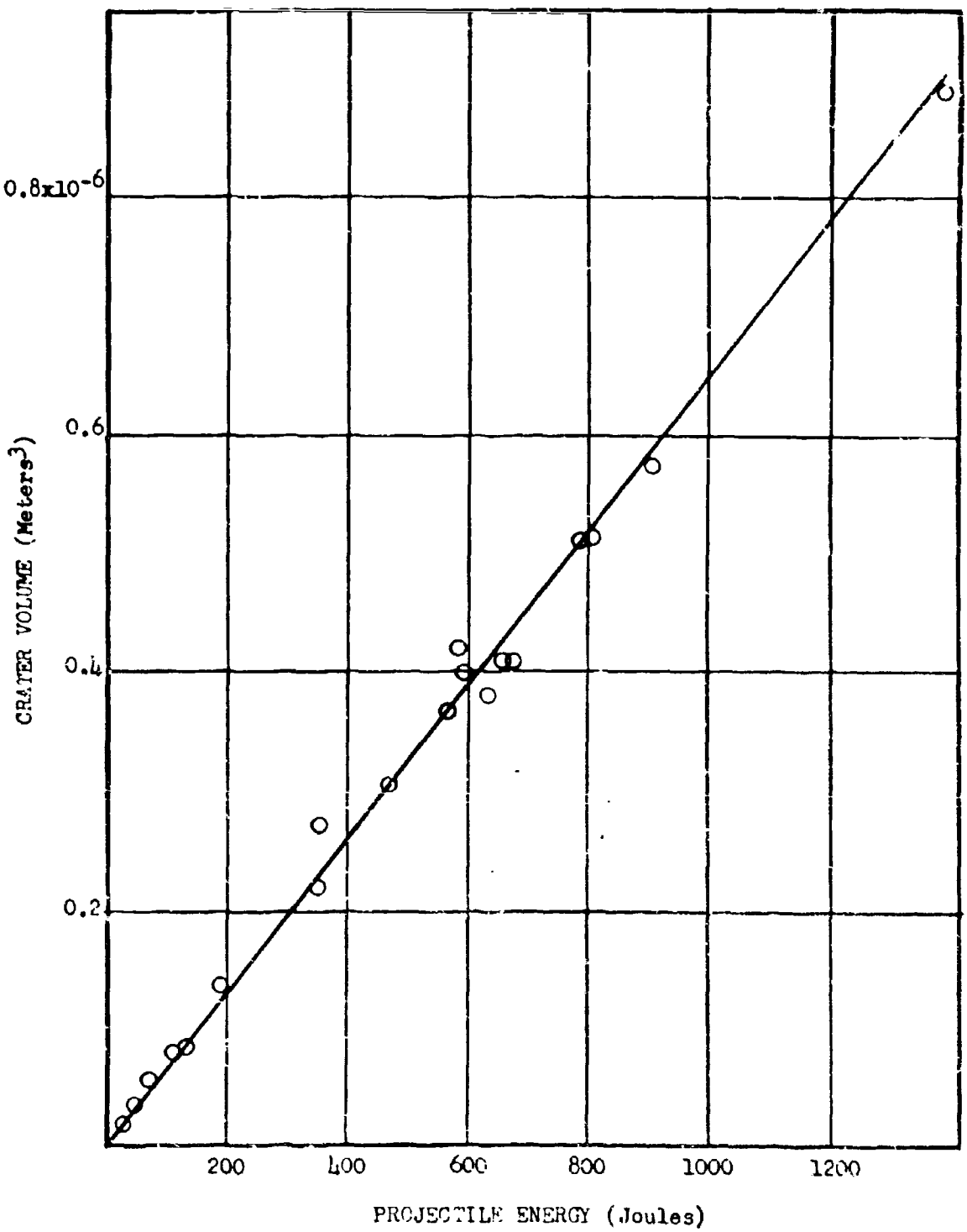

Fig. 20. - Crater volume versus projectile energy for RC-66 steel impacted into zinc.

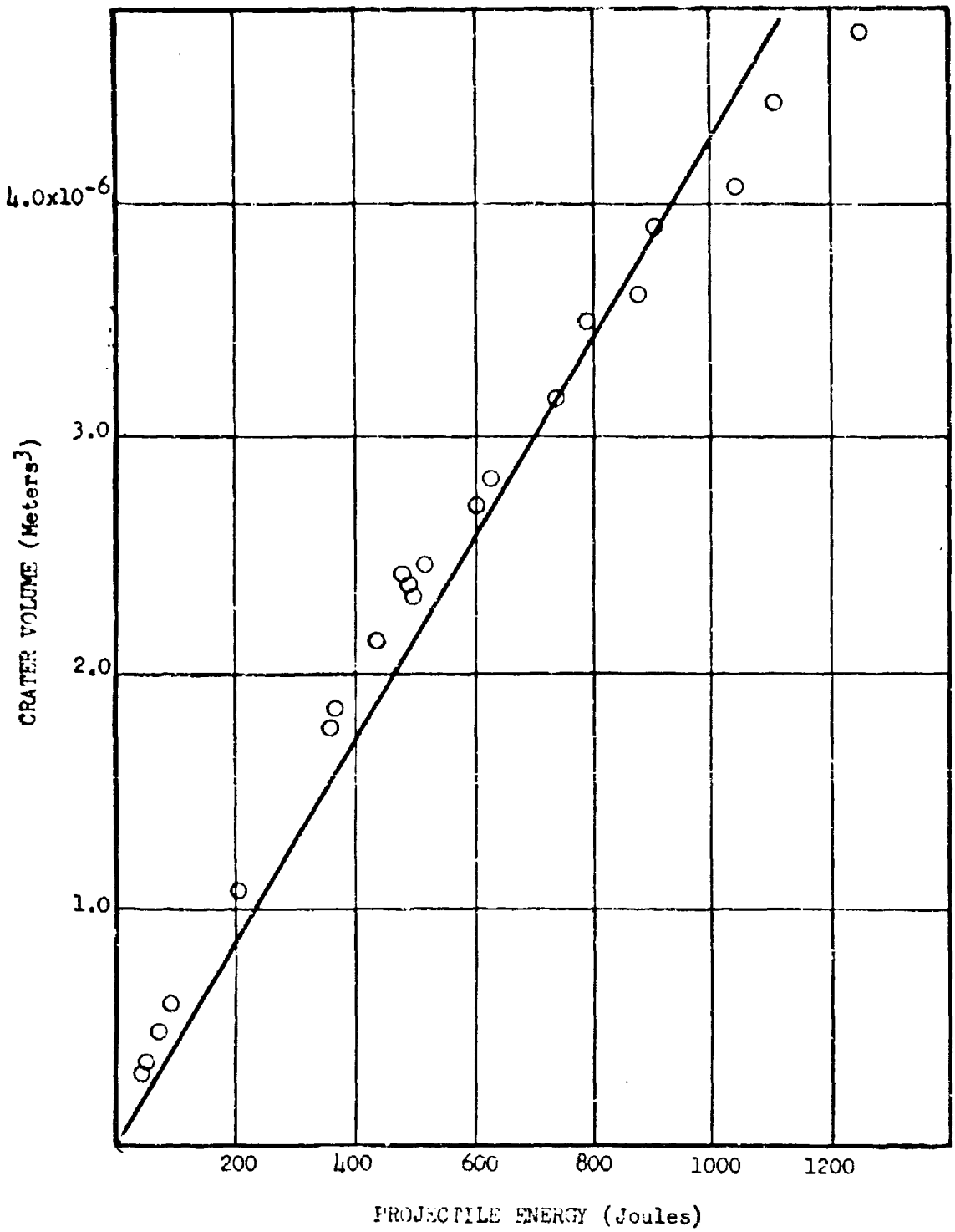

Fig. 21. - Crater volume versus projectile energy for RC-66 steel impacted into lead.

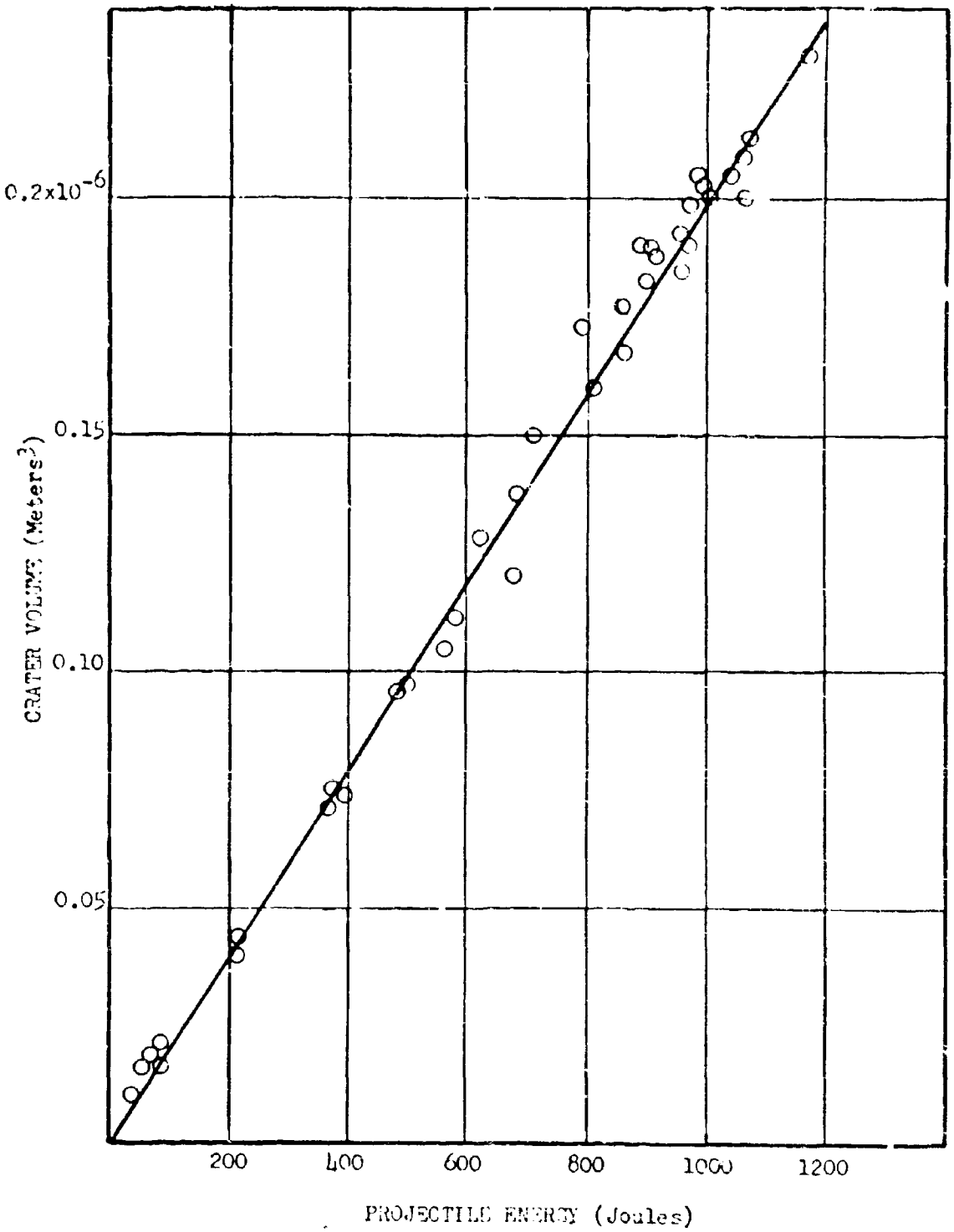

Fig. 22. - Crater volume versus projectile energy for RC-66 steel impacted into 4140 steel.

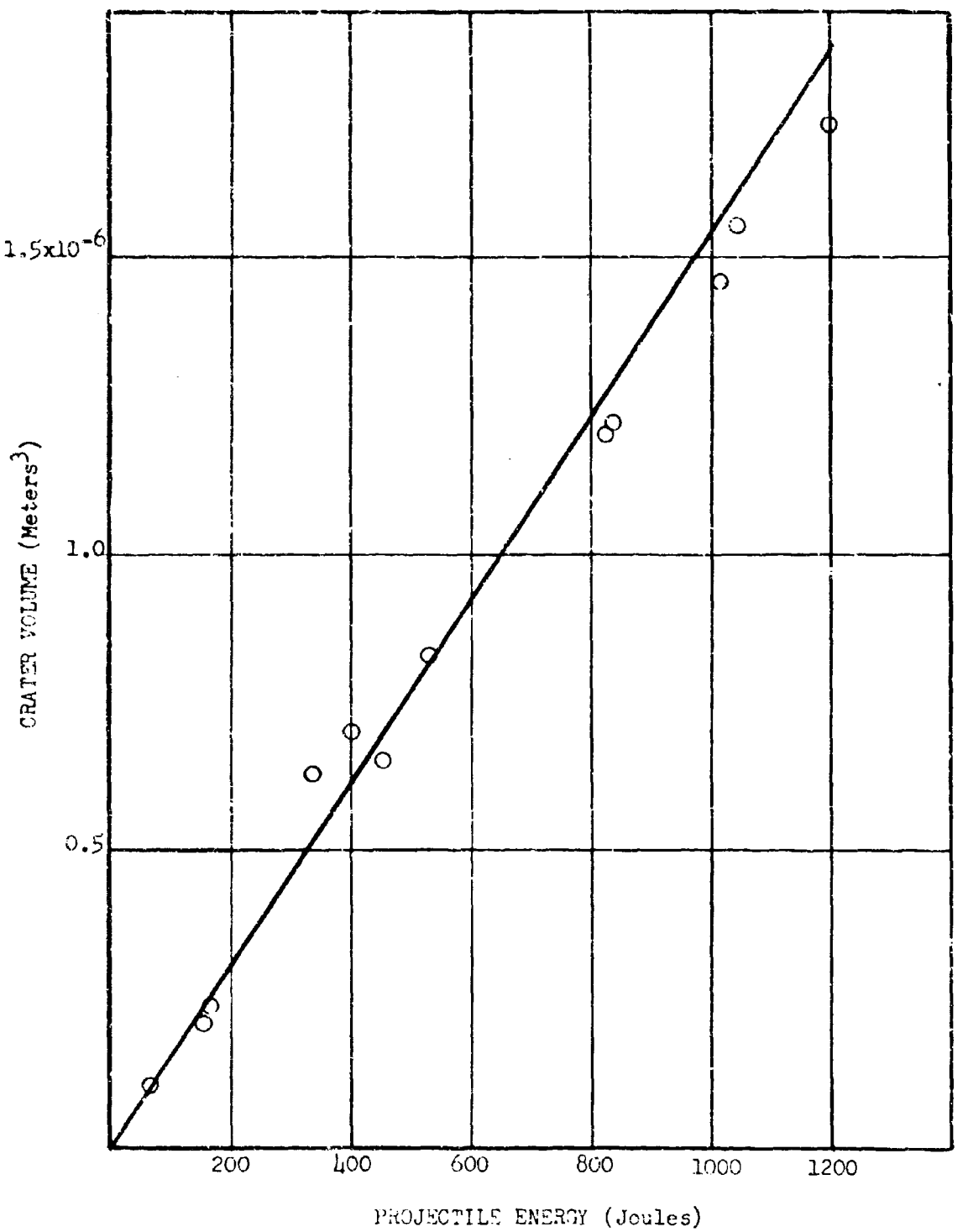

Fig. 23. - Crater volume versus projectile energy for annealed steel impacted into aluminum.

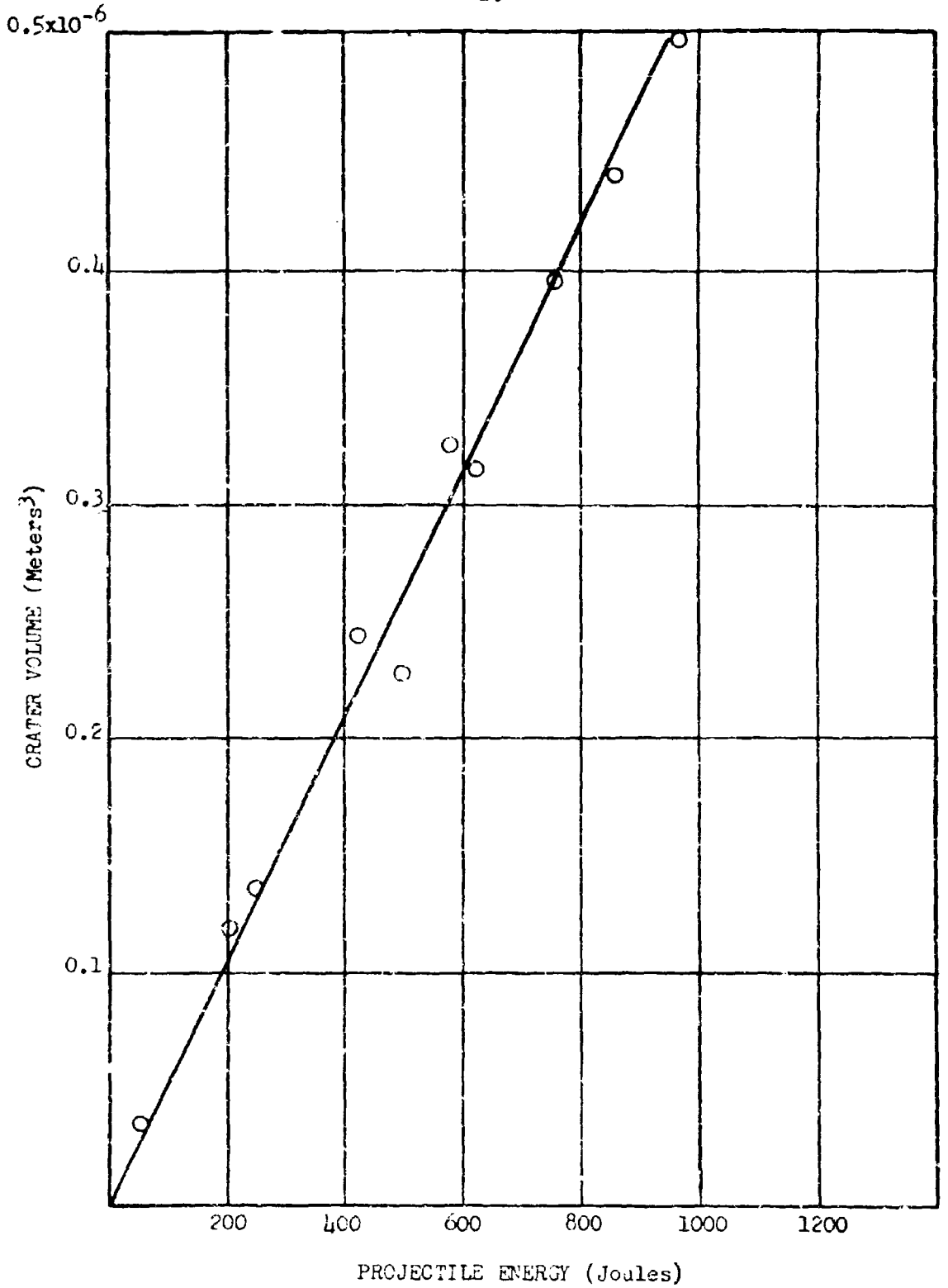

Fig. 24. - Crater volume versus projectile energy for annealed steel impacted into copper.

Crater Area

When crater area is plotted as a function of the momentum of the RC-66 steel projectile, two regions of linearity are found. Figures 25 thru 31 are plots of crater area versus initial impact momentum of the projectile. The point at which the slope changes corresponds to the momentum or velocity at which the projectile was observed to fracture. As has been previously pointed out, the approximate fracture velocity of the projectiles can be determined from the photographs of the cross sectioned craters (Figs. 7 thru 15). The cross section of the craters becomes broader after the fracture velocity is reached. For example, observation of Fig. 8 for RC-66 steel into aluminum indicates the projectile fractures between 1.59 and 1.83 kilometers per second. The slope change for the RC-66 steel into aluminum occurs at 0.75 kgm/sec or 1.7 kilometers per second. Inspection of the cross sectioned copper craters (Fig. 10) impacted with RC-66 steel indicates the fracture of the steel occurs between 0.82 and 1.1 kilometers per second. The change of slope occurs at 0.425 kgm/sec or 0.96 kilometers per second. This relationship between the change of slope and fracture velocity exists for all the target metals tested.

If the velocity at which the slope changes is taken as the fracture velocity of the RC-66 steel projectiles, an interesting relationship exists between it and the target density. Target density versus fracture velocity of the RC-66 steel projectiles is shown in Fig. 32 on page 42. The empirical curve

$$V_f = 8.7 \times 10^4 \rho^{-\frac{1}{2}} \qquad (1)$$

is also shown plotted on Fig. 32 and is seen to fit the experimental

points well. In Eq. (1) V_f is the fracture velocity of the RC-66 steel projectiles in meters per second, and ρ is the target density in kilograms per cubic meter. The fact that the fracture velocity of the RC-66 steel projectiles appears to vary inversely with the square root of the target density can be shown to indicate that the pressure on the projectile is caused by a hydrodynamic mechanism. This inverse relationship can be obtained from a consideration of Bernoulli's equation as applied to an incompressible ideal fluid.[10]

Neglecting the ambient pressure, the stagnation pressure P_s on an object in a fluid is:

$$P_s = \tfrac{1}{2}\rho V^2 \tag{2}$$

where ρ is the fluid density, and V is the relative velocity between the object and the fluid. In the case under consideration, the fluid is the target, and the object in the fluid is the steel projectile. Solving for V, yields:

$$V = (2P_s)^{\frac{1}{2}}\rho^{-\frac{1}{2}}. \tag{3}$$

If this is the mechanism that causes the pressure on the projectile, the stagnation pressure on the RC-66 steel projectile at the fracture velocity is:

$$(2P_s)^{\frac{1}{2}} = 8.7\text{x}10^4 \tag{4}$$

$$P_s = 3.8\text{x}10^9 \text{ newtons/m}^2. \tag{5}$$

The static ultimate tensile stress of the steel in these projectiles is $1.9\text{x}10^9$ newtons/m^2.[11] The stagnation pressure is double the ultimate

stress of the steel. There are various possible explanations why the stagnation pressure is not the same as the ultimate stress of the steel projectile. One is that the stagnation pressure for flow in a metal may not be given exactly by Bernoulli's equation. Another is that the ultimate stress of the steel is increased[12] under the dynamic conditions of cratering. A third possibility is that the geometric configuration of the steel ball increases the ultimate strength over that measured by conventional methods in testing machines.

If the initial linear segment is extrapolated for all the area versus momentum curves, they appear to have an intercept on the crater area axis. This is not the case, for it is impossible to have an area for zero momentum. Instead, the area rises abruptly but not instantaneously to approximately 0.08 meters^{2}x10^{-4} for all the targets. This area is due to the sphere simply leaving its impression on the target.

When crater area is plotted as a function of the projectile momentum for annealed steel into aluminum and copper, the same basic relationships are found to exist as were found for the RC-66 steel projectiles. The results for the annealed steel and the RC-66 steel are both plotted in Figs. 25 and 26. Again there are two linear regions or segments. The intersection of the segments corresponds to the momentum or velocity at which the annealed steel spheres were observed to noticeably deform. The approximate velocity at which deformation begins can also be determined from the photographs of the cross sectioned craters (Figs. 9 and 11). The cross section became broader at the deformation velocity.

From Figs. 25 and 26 it may be seen that the slope of the linear segments for crater area versus projectile momentum are the same for RC-66 steel and annealed steel projectiles impacted into copper and

aluminum. In copper the results for the two steel projectiles appear to be identical. For aluminum, the results are identical for the initial linear segment, but the second linear segment for the annealed steel is displaced from the RC-66 steel segment.

The above relationships for RC-66 steel and annealed steel into copper and aluminum motivated an investigation into the results of other projectile materials impacted into copper and aluminum. Partridge, VanFleet, and Whited[1] in their report present relevant data not only for aluminum impacted into aluminum and copper into copper but also for zinc into zinc and lead into lead. The data for crater area versus projectile momentum from their report are shown plotted on the same graph as the RC-66 steel and annealed steel results in Figs. 25 thru 28. Partridge, VanFleet, and Whited also give data for two sizes of copper projectiles. The copper projectiles were spheres having diameters of 0.38 and 0.483 centimeters. The aluminum, lead, and zinc projectiles were spheres having a diameter of 0.483 centimeters. The steel spheres used for projectiles had a diameter of 3/16 inch or 0.476 centimeters.

Observation of Figs. 25 thru 28 indicates that the slope of the crater area versus projectile momentum curve is the same after deformation of the projectile regardless of the projectile material. At least, parallel lines are consistant with the available data. The results are not as conclusive for lead as they are for copper, zinc, and aluminum.

For the two steel projectiles, there are two linear regions for crater area versus projectile momentum. The initial linear segments are identical. From the data available, one cannot determine if there are two linear regions for the copper, aluminum, and zinc projectiles. If there is an initial segment for the copper, aluminum, and zinc

projectiles, and if the earlier discussed hydrodynamic mechanism causes the pressure on the projectiles; the velocity at which the initial and final segments intersect is determined by the strength of the projectile. The pressure at which the aluminum projectiles fails is low. This is the reason the aluminum into aluminum line on Fig. 25, if extrapolated to zero momentum, nearly passes through the origin.

Another interesting fact comes from the smaller copper projectiles in Fig. 26. The smaller spheres produce the same slope for crater area versus projectile momentum as the larger copper projectiles do. For that matter, it is the same slope that the two steel projectiles produce. The 0.38 cm copper projectile results are displaced from the 0.483 cm copper and steel results, however.

The values for slope of the initial segment and the final segment for the targets are given in Table 2. The sequence of targets for final crater area versus projectile momentum is the same as the sequence for crater volume versus projectile energy. Thus, it appears that the same factors that influence the volume per unit energy also influence the crater area per unit momentum after deformation or fracture of the projectiles.

Table 2. - Experimental values of initial and final slope for crater area versus projectile momentum and crater volume per unit energy. Targets were all impacted with RC-66 steel projectiles.

Target Material	Initial Slope	Final Slope	$\frac{\text{Volume}}{\text{Energy}}$
Lead	2.65×10^{-4} m^2/kgm/sec	6.65×10^{-4} m^2/kgm/sec	4.25×10^{-9} m^3/joule
Aluminum	0.62×10^{-4}	2.63×10^{-4}	1.67×10^{-9}
Silver	0.53×10^{-4}	2.31×10^{-4}	0.86×10^{-9}
Magnesium	0.35×10^{-4}	2.00×10^{-4}	0.84×10^{-9}
Zinc	0.68×10^{-4}	1.82×10^{-4}	0.65×10^{-9}
Copper	0.45×10^{-4}	1.48×10^{-4}	0.60×10^{-9}
4140 Steel	0.41×10^{-4}	0.87×10^{-4}	0.20×10^{-9}

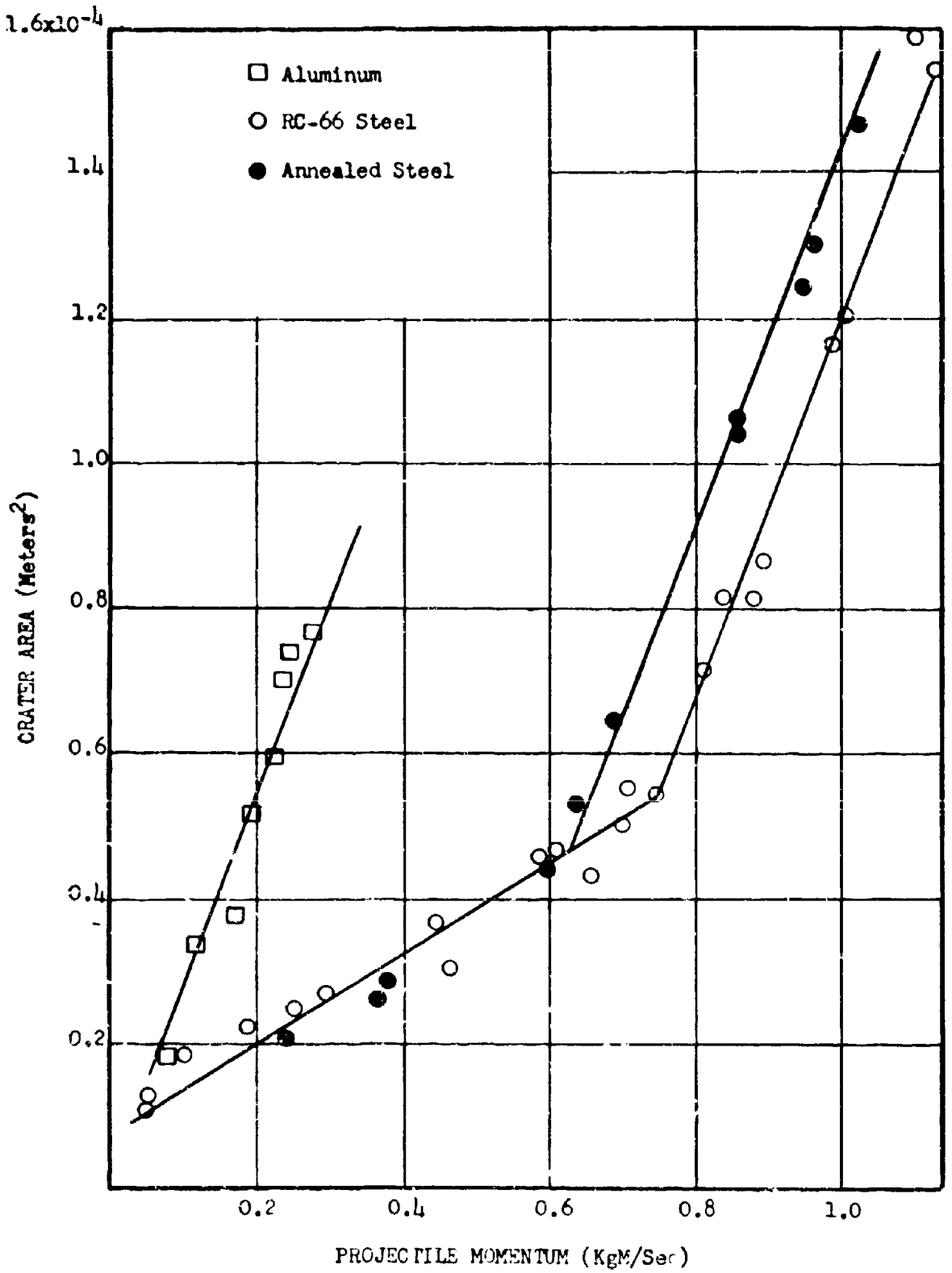

Fig. 25. - Crater area versus projectile momentum for RC-66 steel, annealed steel, and aluminum impacted into aluminum.

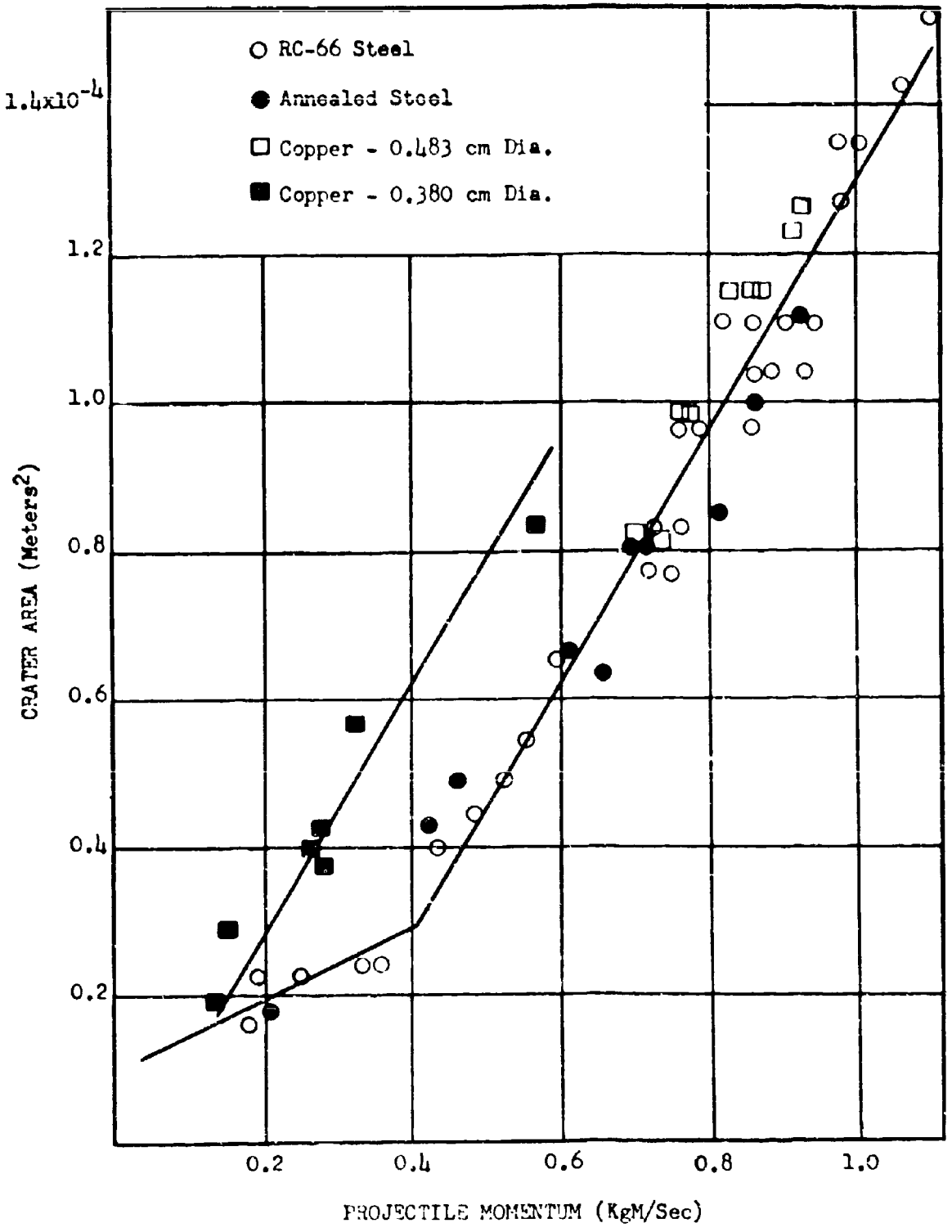

Fig. 26. - Crater area versus projectile momentum for RC-66 steel, annealed steel, and copper impacted into copper.

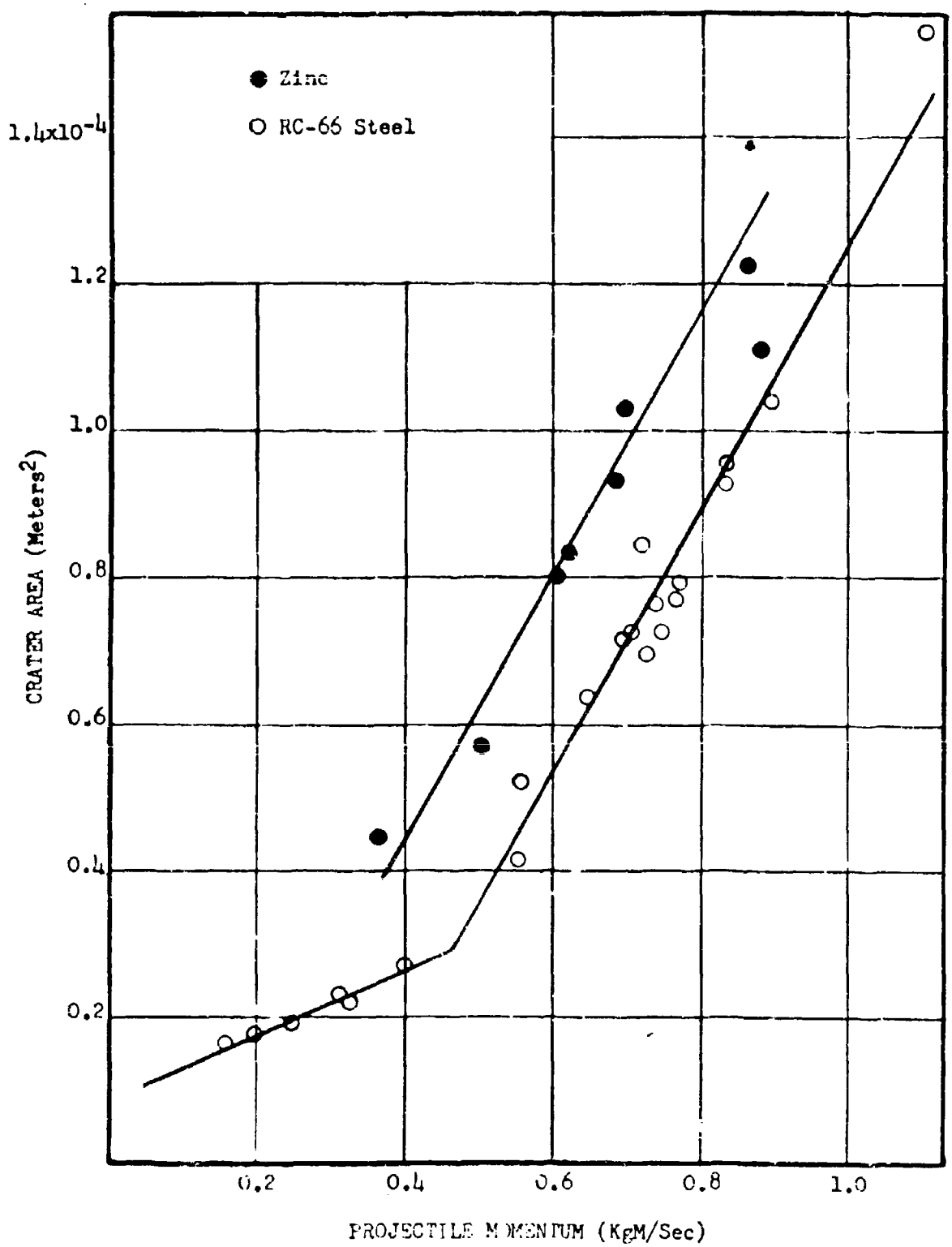

Fig. 27. - Crater area versus projectile momentum for RC-66 steel and zinc impacted into zinc.

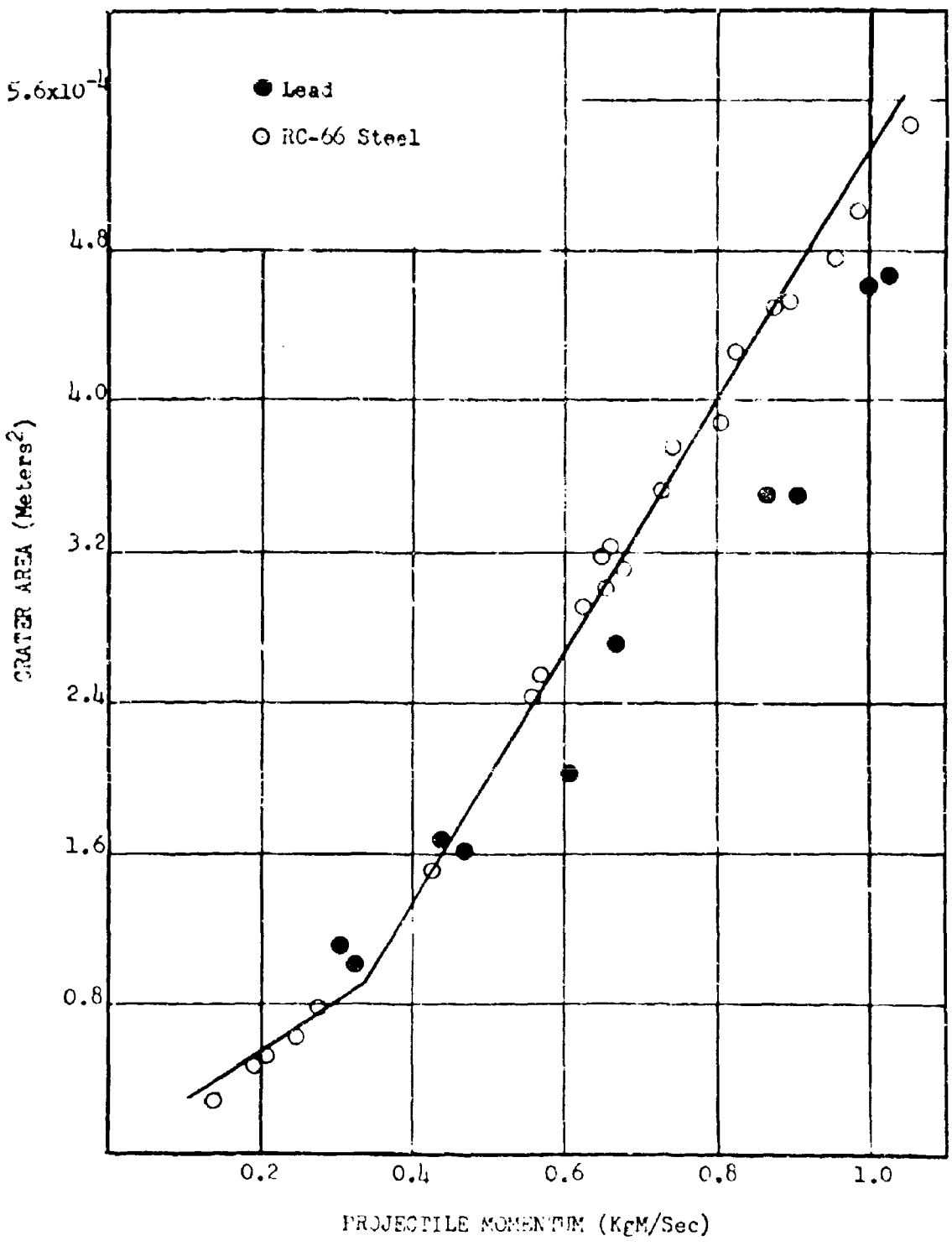

Fig. 28. - Crater area versus projectile momentum for RC-66 steel and lead impacted into lead.

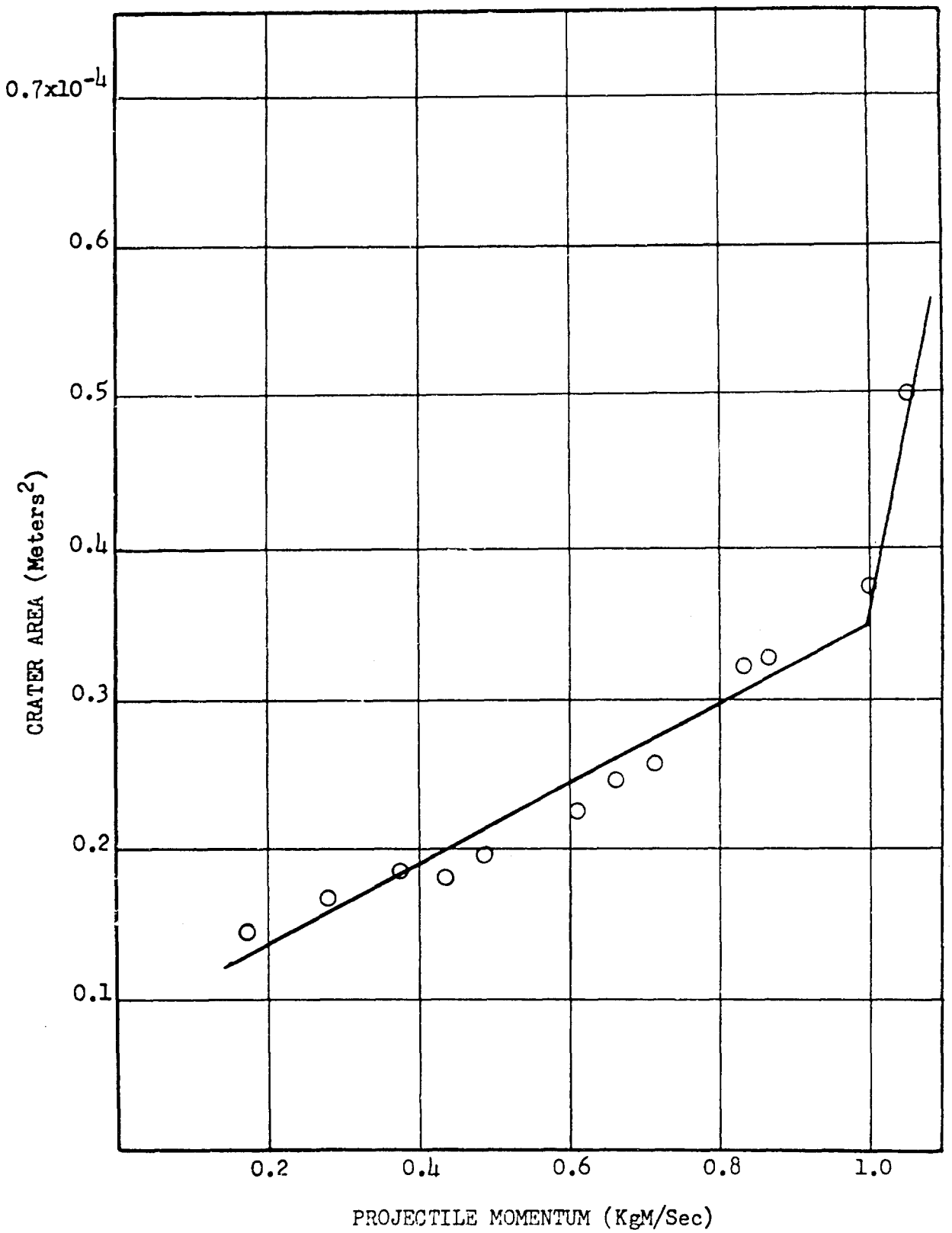

Fig. 29. - Crater area versus projectile momentum for RC-66 steel impacted into magnesium.

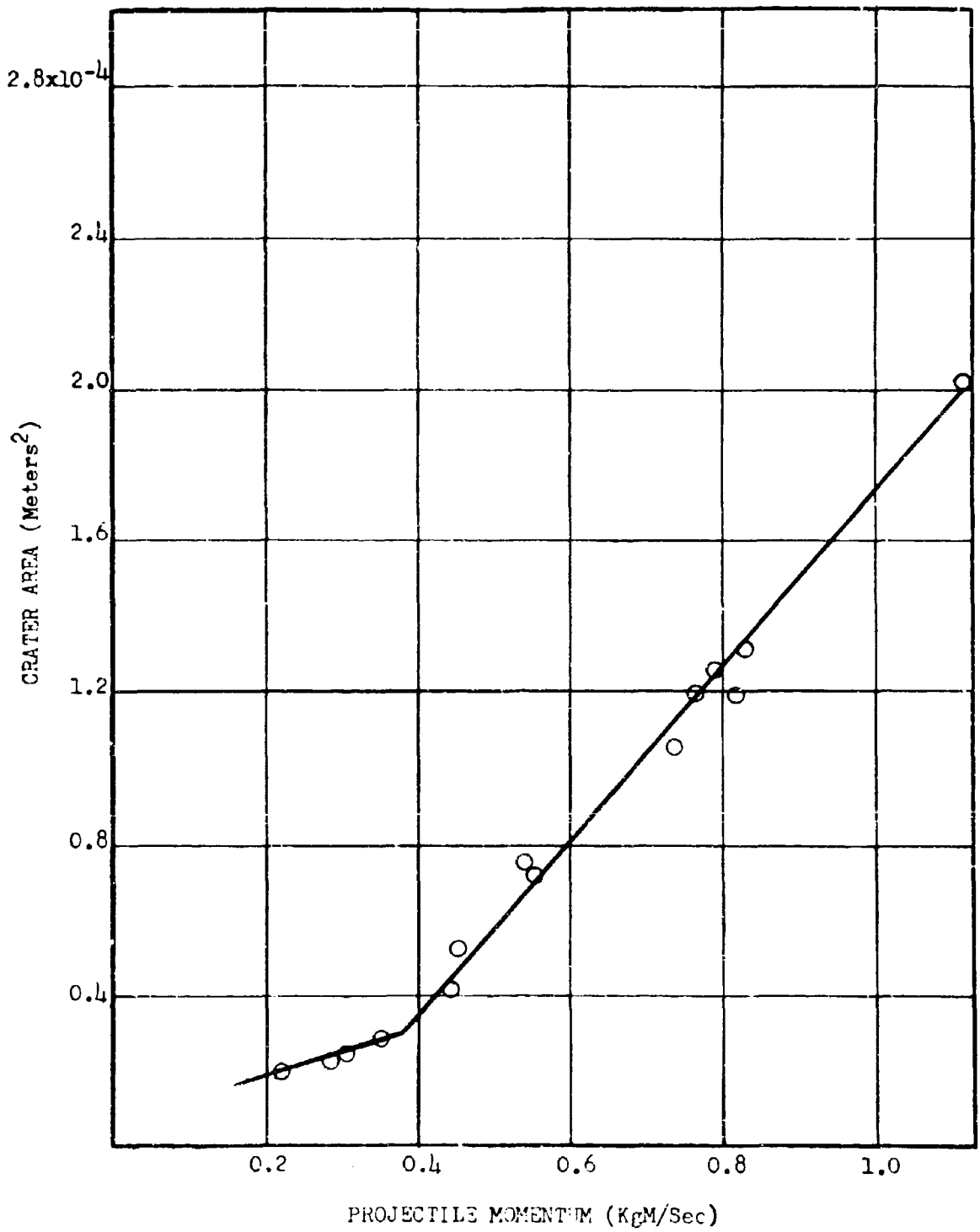

Fig. 30. - Crater area versus projectile momentum for RC-66 steel impacted into silver.

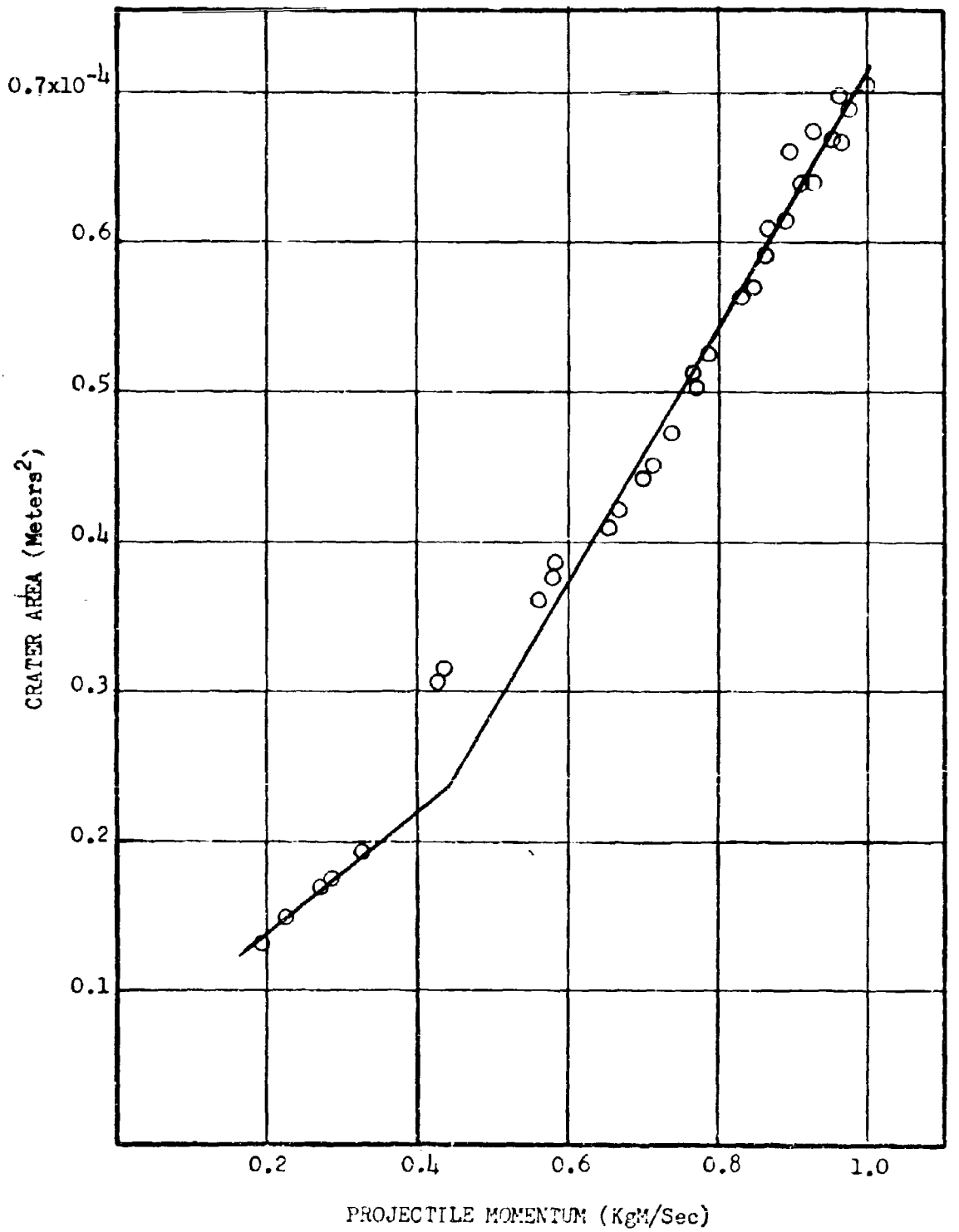

Fig. 31. - Crater area versus projectile momentum for RC-66 steel impacted into 4140 steel.

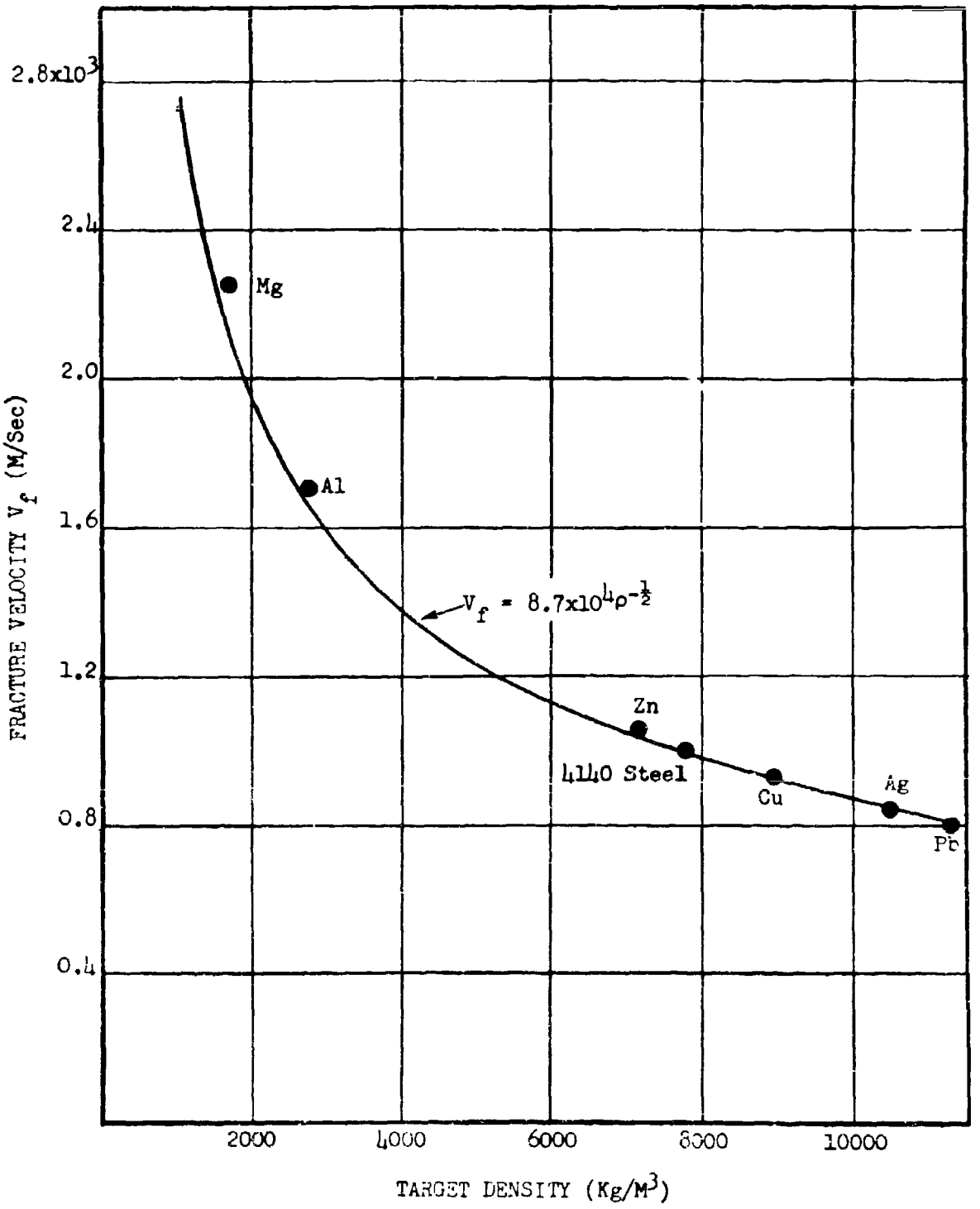

Fig. 32. - Fracture velocity versus target density for RC-66 steel projectiles.

Penetration

Crater volume versus projectile energy and crater area versus projectile momentum had similar plots for all the targets. No such similarity could be found for all the targets for the penetration parameter. Penetration as a function of the projectile momentum is shown on Figs. 33 thru 41 for the targets under consideration. The penetration data are more erratic than either the volume or area data. One may question the validity of drawing straight line segments for penetration versus momentum as was done. Other continuous curves could be drawn through most of the data; however, the straight line segments approximate the available data well in most cases.

Probably the most interesting fact that came from the penetration parameter plots is observed in aluminum, lead, and magnesium. In these three targets a region is found where penetration decreases for an increase in momentum (see Figs. 33, 34, 35, and 36). This decrease also can be observed from the photographs of the cross sectioned craters in Figs. 8, 9, 12, and 13. This decrease in penetration starts at about the same momentum that the slope change occurs on the crater area-momentum plots. The penetration in aluminum by RC-66 steel can be observed from Fig. 33 to start to decrease at about 0.72 kgm/sec. From Fig. 25 for crater area versus momentum for the RC-66 steel projectiles into aluminum, the slope change occurs at about 0.75 kgm/sec. From Fig. 35 the penetration in magnesium is seen to start to decrease at about 0.95 kgm/sec; the momentum where the slope changes for crater area versus momentum in magnesium is at about 0.98 kgm/sec (see Fig. 29). The penetration starts to decrease in lead at about 0.3 kgm/sec (see Fig. 36), and the slope change on Fig. 28 occurs at about 0.35 kgm/sec. This same

relation can be seen to exist for annealed steel impacted into aluminum (see Figs. 25 and 34). At higher momentums, the penetration in lead resumes a positive slope. In the velocity range covered this cannot be definitely observed for either the magnesium or aluminum targets. Aluminum may be just on the verge of resuming a positive slope.

The data of penetration versus projectile momentum for zinc, silver, and copper impacted with RC-66 steel can be approximated with two straight lines as shown in Figs. 37, 38, and 39. These three targets have similar plots as do the aluminum, lead, and magnesium. Zinc, silver, and copper do not have a region where there is a decrease in penetration for an increase in momentum. Instead, the slope of penetration versus momentum decreases (but remains positive) after a certain momentum. This momentum approximately corresponds to the momentum at which the slope changes in a plot of crater area versus projectile momentum. For example the penetration slope starts to decrease in zinc at about 0.41 kgm/sec (see Fig. 37), and the slope change for crater area versus momentum occurs at about 0.47 kgm/sec (see Fig. 27). This same relationship can be observed to exist for copper and silver impacted with RC-66 steel projectiles (compare Figs. 38 and 26 and Figs. 39 and 30 respectively).

Figures 40 and 41 are plots of penetration versus projectile momentum for 4140 steel impacted with RC-66 steel and copper impacted with annealed steel. As can be observed from the graphs, they both appear to be linear. At least the data can be approximated with one straight line.

It has been shown that the momentum where the slope changes on the plots of crater area versus momentum corresponds to the momentum or

velocity at which there is noticeable deformation or fracture of the steel projectile. It has also been shown that the slope change on the crater area versus projectile momentum plot and the slope change of the penetration versus projectile momentum plot occur at approximately the same momentum. Thus, the slope of penetration versus momentum becomes less after the projectile deforms or fractures. The slope becomes negative for aluminum, magnesium, and lead; and the slope decreases for copper, zinc, and silver impacted with RC-66 steel.

If the projectile is able to retain its spherical shape upon impact, the crater will be long and narrow. This fact can be observed from the cross sectioned craters. This is especially noticeable in aluminum and magnesium (compare Fig. 8, 9, and 12). If the projectile fractures or is noticeably deformed, it presents more area to the target. As a result, the penetration decreases, and the area increases. Since it has been shown that the fracture velocity of the RC-66 steel projectiles varies inversely with the target density, one would expect the deepest craters in the material with the smallest density. This is observed to be the case except in lead where other nonapparent factors may be dominating. Magnesium has a density of 1.7 gm/cm^3 and has a maximum penetration for the velocity range covered of about 3.4×10^{-2} meters. Aluminum has a density of 2.74 gm/cm^3 and a maximum penetration of about 2.8×10^{-2} meters for the velocity range under consideration. The penetration in lead is next with the other targets considerably less.

Striations in Craters

An observation worthy of note was made in silver, copper, and the 4140 steel craters. When the projectile fractured or deformed upon impact in these metals, a small impression or dent was made in the bottom

(generally in the center) of the craters. The impression was circular having a diameter of between 1 or 2 millimeters. Occasionally, this impression contained a small steel fragment. If this steel fragment were removed, this small circular impression remained. Inside the impression scratches or striations were observed. These striations were oriented in the same direction as the machine marks from a lathe on the surface of the target. A few of the steel fragments that were in the impression were recovered; they had the same striations as the impression. These observations give indications that the metal in the impression was originally on the surface of the target and was merely compressed undeformed to the bottom of the crater. Since the steel fragment, sometimes observed in the impression, also had striations, another possibility is that the surface of the target left its impression on the leading edge of the projectile which in turn left an impression on the target metal in front of the leading edge when the leading edge finally stopped.

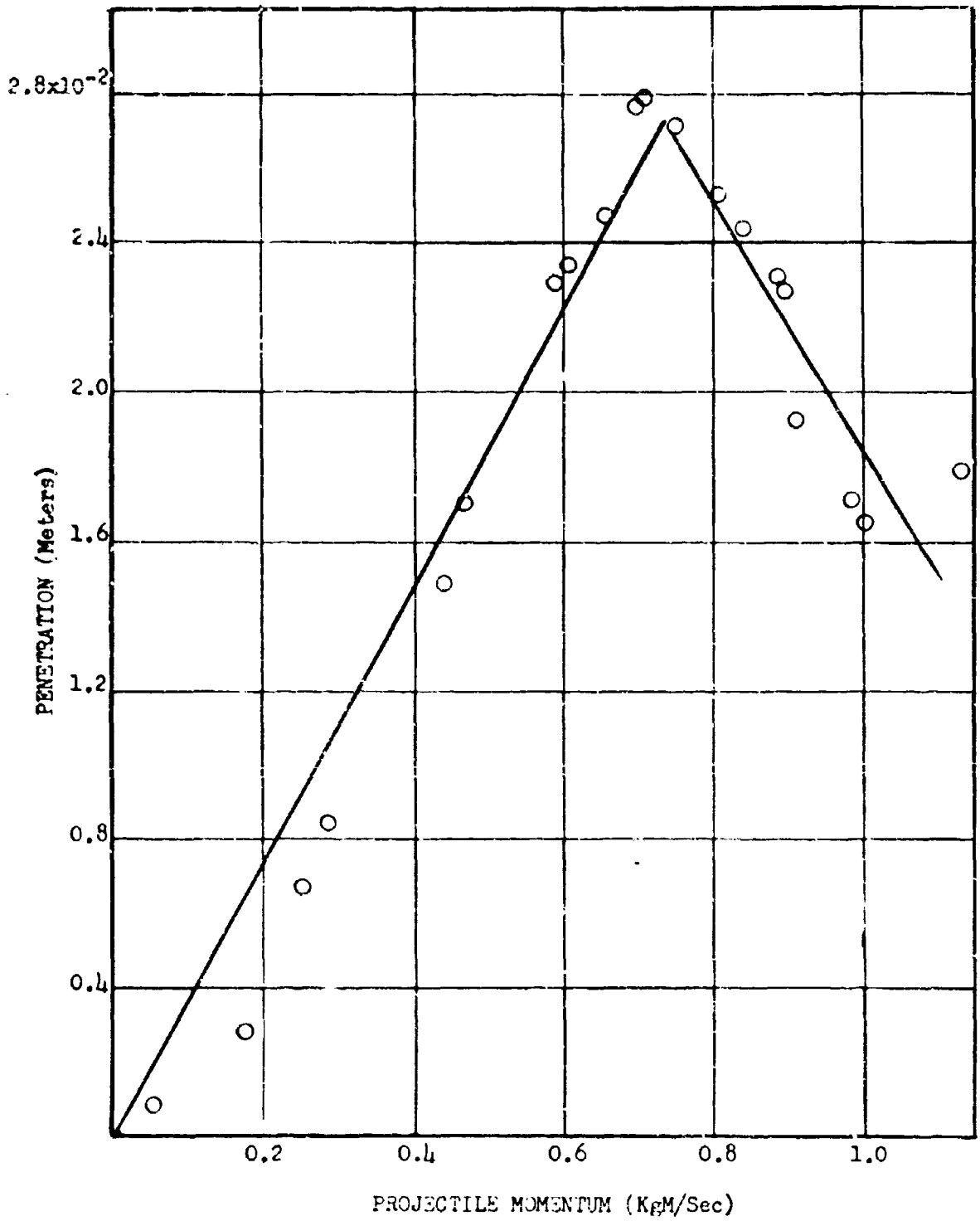

Fig. 33. - Penetration versus projectile momentum for RC-66 steel impacted into aluminum.

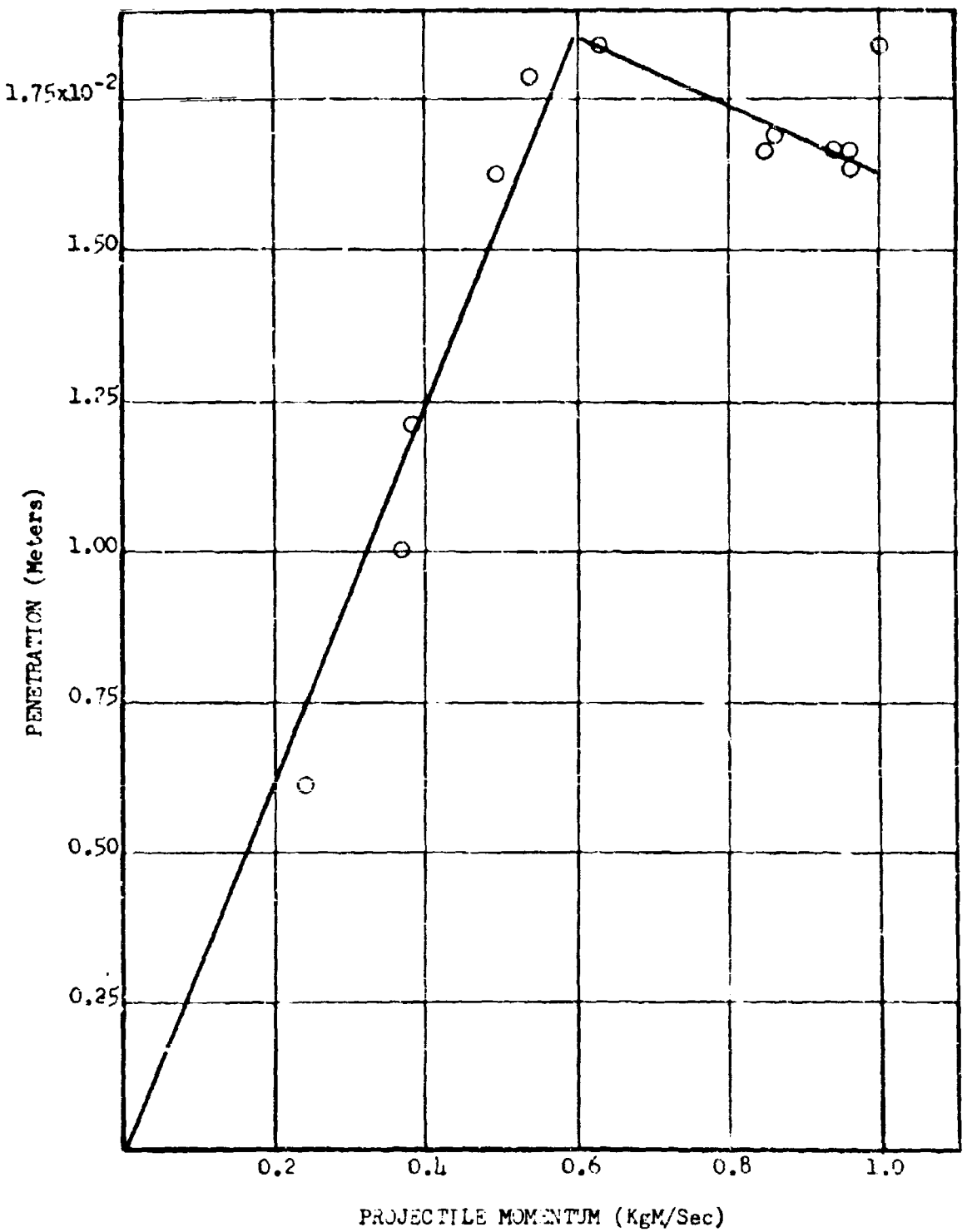

Fig. 34. - Penetration versus projectile momentum for annealed steel impacted into aluminum.

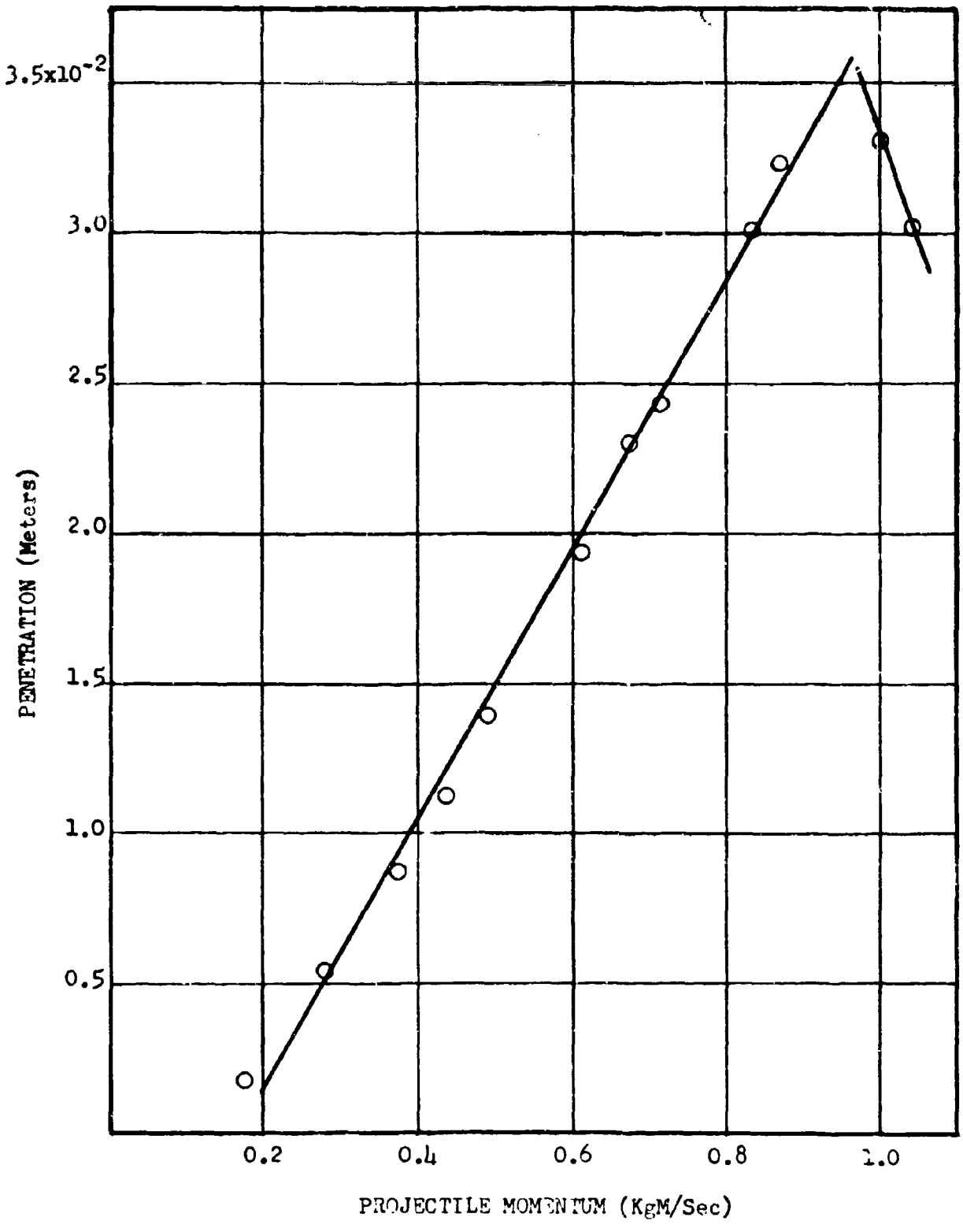

Fig. 35. - Penetration versus projectile momentum for RC-66 steel impacted into magnesium.

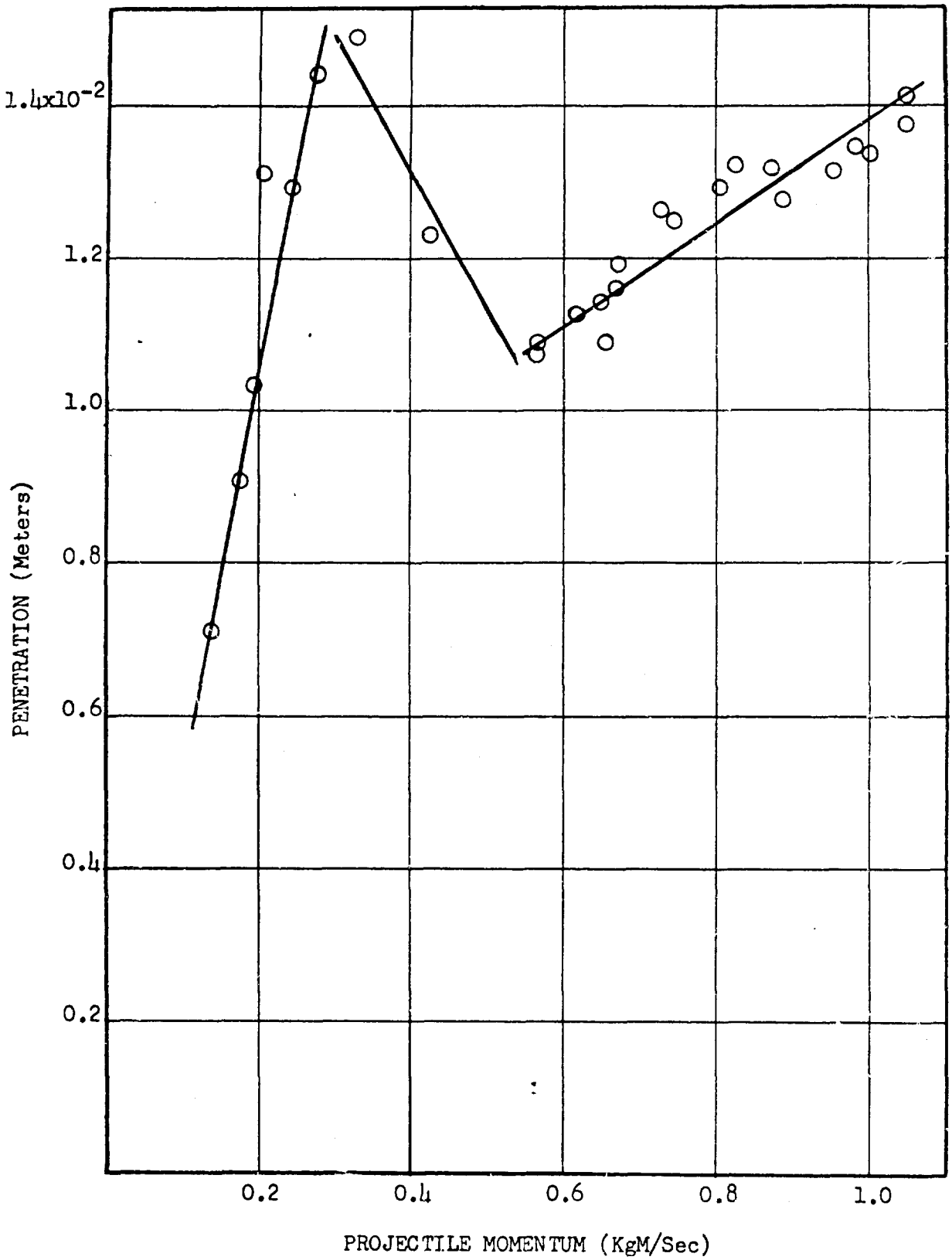

Fig. 36. - Penetration versus projectile momentum for RC-66 steel impacted into lead.

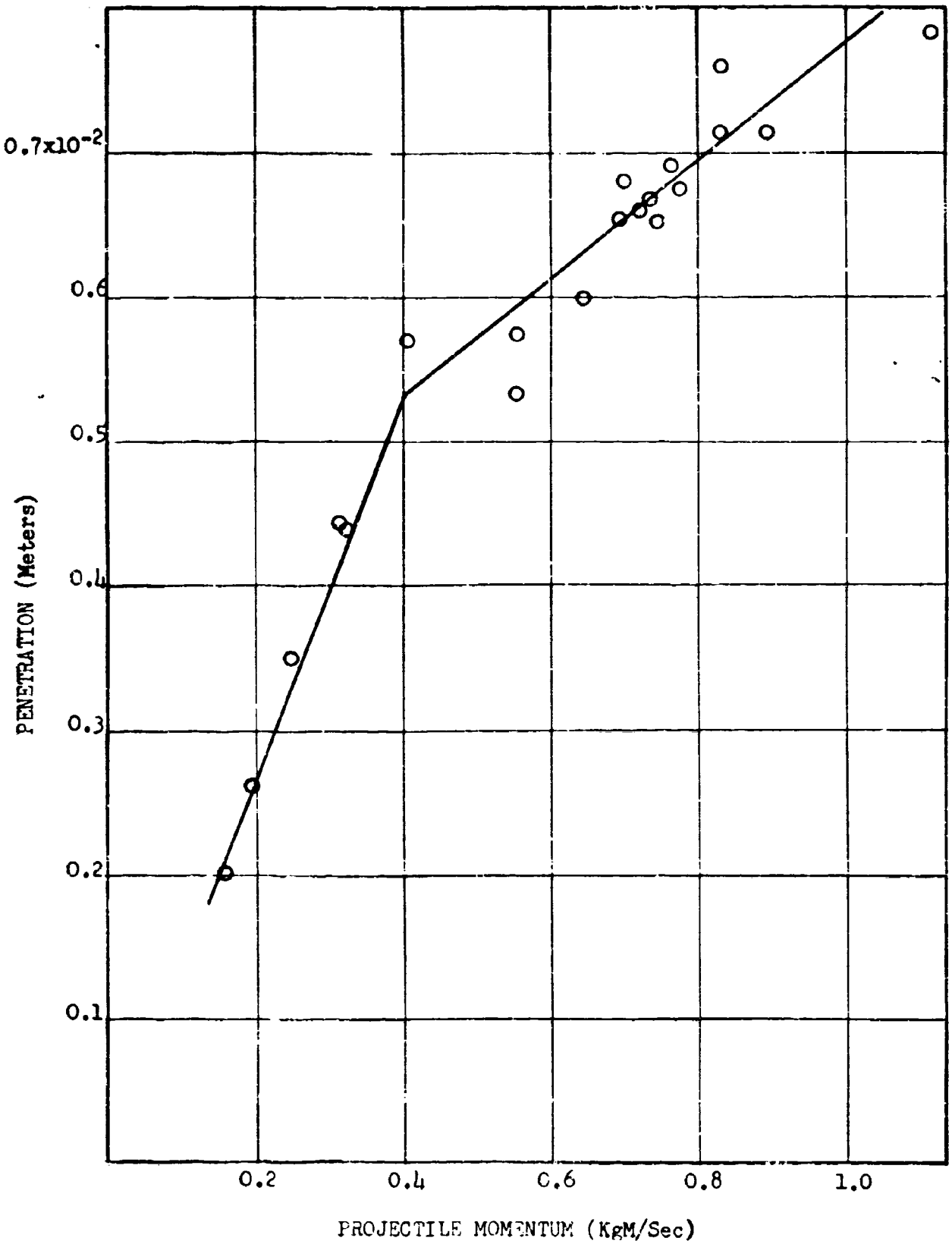

Fig. 37. - Penetration versus projectile momentum for RC-66 steel impacted into zinc.

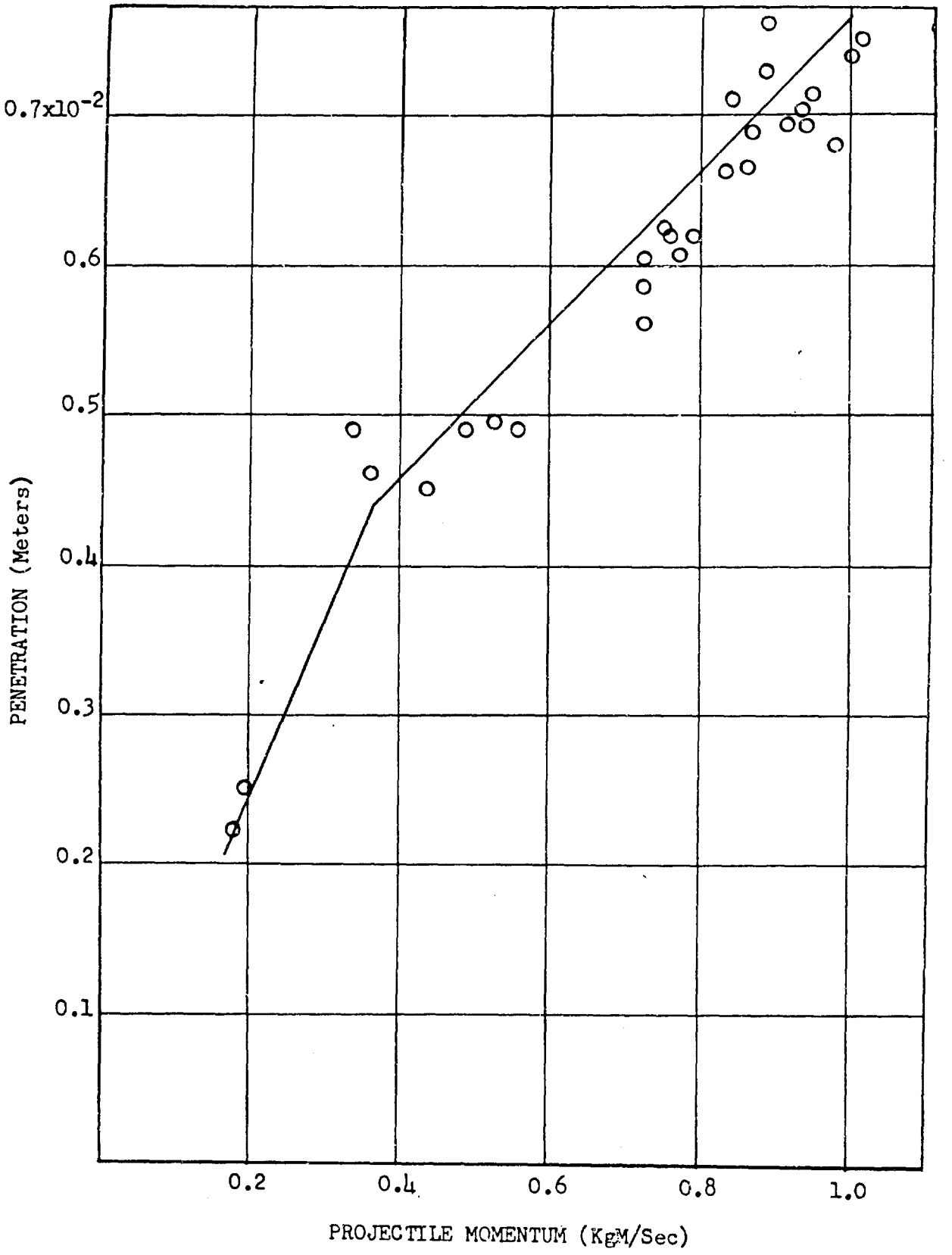

Fig. 38. - Penetration versus projectile momentum for RC-66 steel impacted into copper.

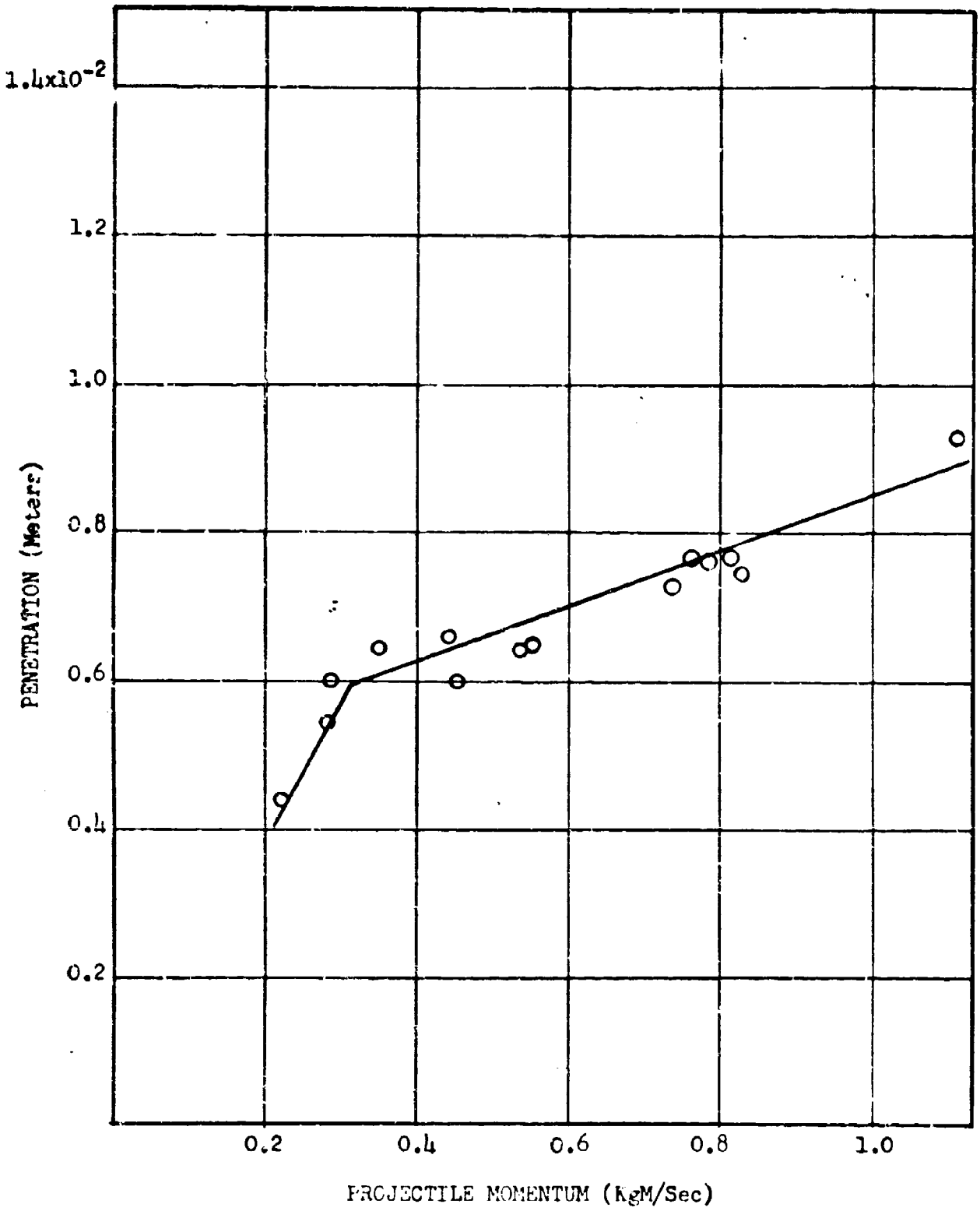

Fig. 39. - Penetration versus projectile momentum for RC-66 steel impacted into silver.

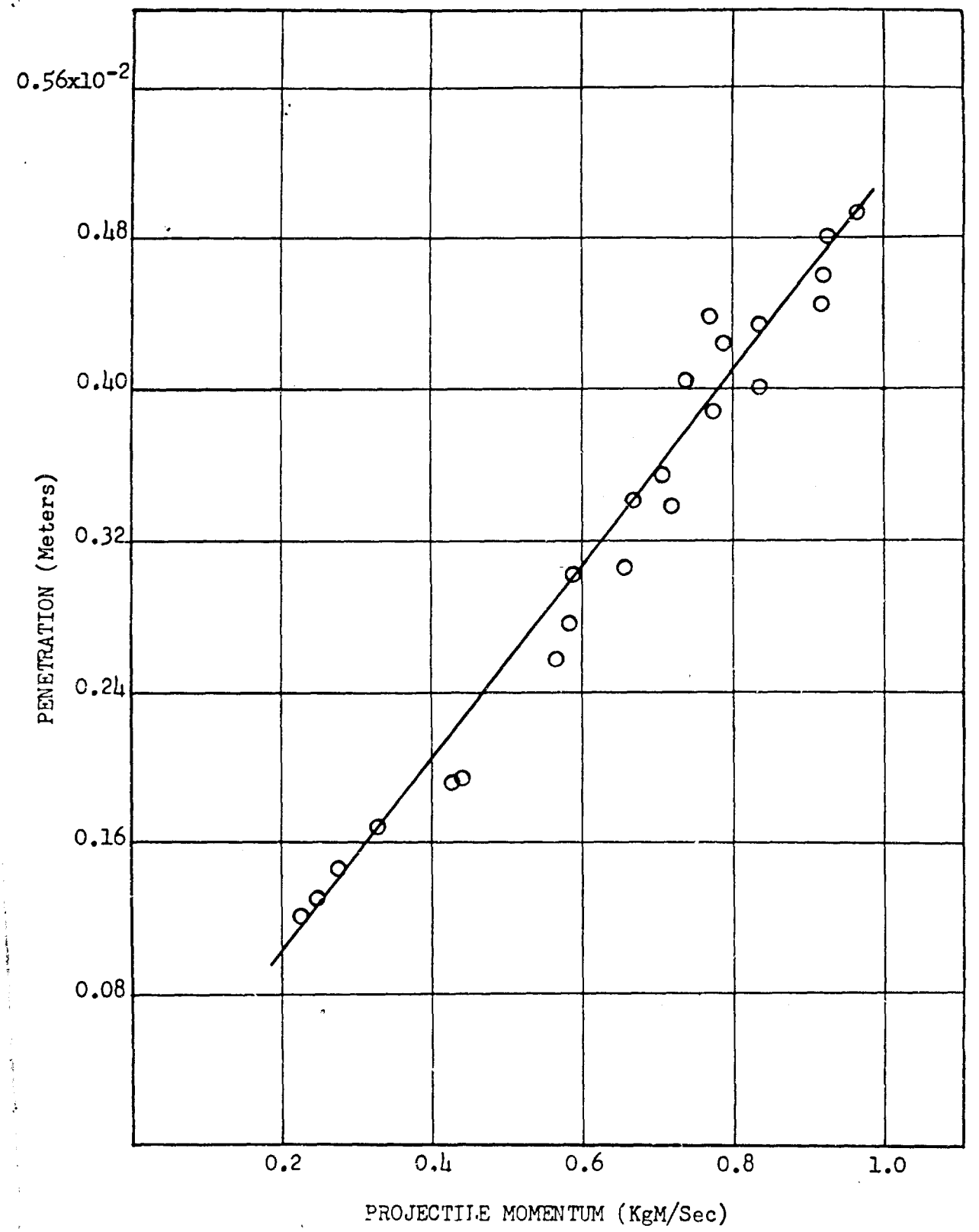

Fig. 40. - Penetration versus projectile momentum for RC-66 steel impacted into 4140 steel.

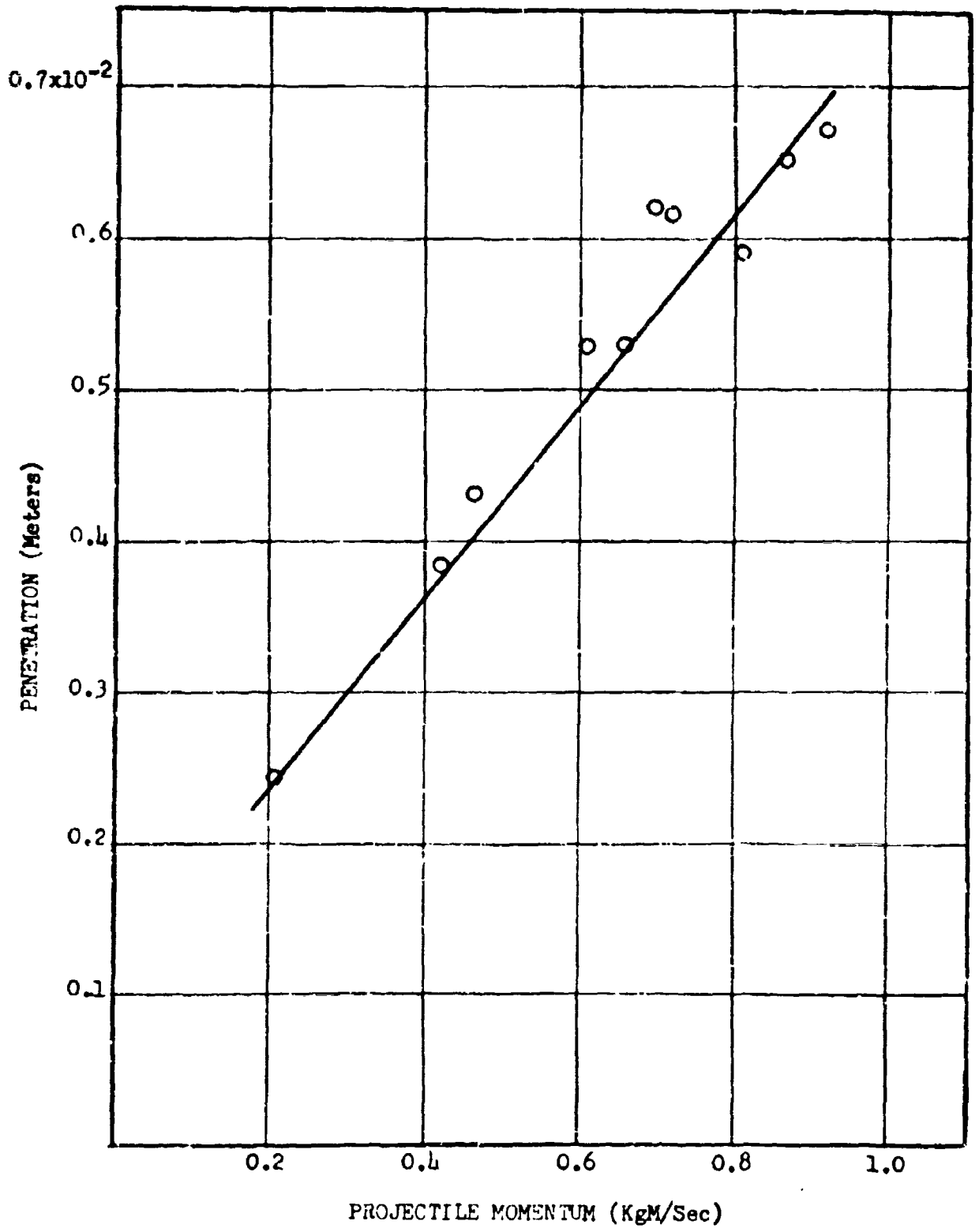

Fig. 41. - Penetration versus projectile momentum for annealed steel impacted into copper.

THEORETICAL CONSIDERATIONS

An expression for the force on the target can be written from a consideration of Newton's second law of motion:

$$F_t = m_p a_p. \tag{6}$$

In Eq. (6), F_t is the force exerted on the target, m_p is the mass of the projectile, and a_p is the acceleration of the projectile after impact. The acceleration a_p can be written as $-dv_p/dt$ where v_p is the velocity of the projectile. Making this substitution and dividing and multiplying by dx, yields:

$$F_t = -m_p \frac{dv_p}{dx} \frac{dx}{dt}. \tag{7}$$

But, dx/dt is the velocity of the projectile v_p. Hence,

$$F_t = m_p v_p dv_p/dx. \tag{8}$$

Integrating Eq. (8) with respect to x:

$$\int_0^{X_o} F_t dx = -\int_{V_o}^{0} m_p v_p dv_p. \tag{9}$$

In Eq. (9), X_o is the depth of the crater, and V_o is the initial impact velocity of the projectile. The right side of Eq. (9) integrates to $\frac{1}{2}m_p V_o^2$. This expression is the initial impact energy which was plotted against crater volume. Thus,

$$\int_0^{X_o} F_t dx = \tfrac{1}{2}m_p V_o^2 = \text{Energy}. \tag{10}$$

The force F_t can be written as a pressure P acting on an area A.

Making the substitution that $F_t = PA$:

$$\int_0^{X_o} PA\,dx = \text{Energy}. \tag{11}$$

The pressure P is a function of the target material, and in the velocity range under consideration it is reasonable to believe that P is constant for a given material. That is, there is a pressure for a given material at which the target will fail. Thus, if P is constant, it can be removed from the integral of Eq. (11):

$$P\int_0^{X_o} A\,dx = \text{Energy}. \tag{12}$$

The question that now arises is what is the pressure P. Two possibilities for P are the shear strength and the yield strength. If P is assumed to be the shear strength P_{ss}, then A in Eq. (10) is the shear area A_s.

Under the assumption that P is the shear strength, Eq. (12) becomes:

$$P_{ss}\int_0^{X_o} A_s\,dx = \text{Energy}. \tag{13}$$

Under the dynamic conditions of impact, the exact area on which the shear pressure acts cannot be specifically determined. It is convenient to make the assumption that the shear area $A_s(x)$ at any distance x from the surface of the target in the crater is directly proportional to the area of the crater $A_c(x)$ at that same distance into the crater.

With the assumption that $A_s(x) = KA_c(x)$, Eq. (13) becomes:

$$P_{ss}K\int_0^{X_o} KA_c(x)\,dx = \text{Energy} \tag{14}$$

$$P_{ss}K\int_0^{X_o} A_c(x)\,dx = \text{Energy}. \tag{15}$$

The expression $\int_0^{X_o} A_c(x)dx$ is simply the crater volume. Thus, Eq. (15) becomes:

$$\frac{\text{Crater Volume}}{\text{Projectile Energy}} = \frac{1}{KP_{ss}}. \tag{16}$$

The values of the shear strength for all the target metals except silver are shown in Table 3. No value could be found for silver. Also shown in Table 3 are the values for K in Eq. (16) for the various metals.

Table 3. - Shear strength for the target materials.

Target Material	Shear Strength	(Shear Strength)$^{-1}$	Constant (K)
Lead[13]	1.2×10^{7} newtons/m^2	83.4×10^{-9} m^3/joule	19.7
Aluminum[13]	6.5×10^{7}	15.4×10^{-9}	9.3
Magnesium[13]	13.0×10^{7}	7.7×10^{-9}	9.2
Zinc[14]	13.1×10^{7}	7.6×10^{-9}	11.7
Copper[13]	15.8×10^{7}	6.3×10^{-9}	10.5
4140 Steel[15]	55.0×10^{7}	1.8×10^{-9}	9.0

From Table 3 it is interesting to note, that with the exception of lead, K is approximately the same with an average value of 10. The reason lead differs is not obvious. Perhaps, there is a nonapparent, different mechanism operating in lead. The values listed for shear strength in Table 3 are all static values. The strength of a material increases as the rate of loading is increased. If the shear strengths were known at the loading rate that accompanies cratering, perhaps the proportionality constant K would be the same for all the metals including

lead. That is, between static and dynamic rates of loading the shear strength in lead may increase more than in the other metals. In the derivation of the volume/energy of Eq. (16), K is the proportionality constant between $A_s(x)$ and $A_c(x)$. (Remember that x is the distance from the surface of the target into the crater.) The possibility exists that $A_s(x)$ is not directly proportional to $A_c(x)$ but is a function of $A_c(x)$. Observation of Figs. 25 thru 31 indicates that, over the velocity range covered, all the metals except lead have a crater area at the surface of the target that ranges up to approximately 1 cm^2. For lead the crater area at the target surface ranges up in the vicinity of 4 cm^2. These two areas (1 cm^2 and 4 cm^2) are that area of the craters at the surface of the target, but they are an indication of the relative magnitude of $A_c(x)$. If $A_s(x)$ is a function of $A_c(x)$, the metals where $A_c(x)$ has about the same magnitude would exhibit a constant relationship between $A_s(x)$ and $A_c(x)$. In lead $A_c(x)$ is about 4 times larger than that of the other targets, and if $A_s(x)$ is a function of $A_c(x)$, then the proportionality between $A_s(x)$ and $A_c(x)$ may be different.

A similar analysis can be made by assuming P to be the yield strength of the target. The yield strength P_{ys} of the actual target materials was measured by loading a cylinder of the target material $\frac{1}{2}$ inch in diameter and 2 inches in length on a Baldwin testing machine at a loading rate of 100,000 lb/min. The compressive yield strengths obtained from the stress-strain diagram by using the 0.35% offset method are shown on Table 4. Also shown on Table 4 is the proportionality constant K that will make $1/KP_{ys}$ equal to the experimentally measured volume per unit energy. As can be observed from Talbe 4, all metals except lead and zinc have approx-

imately the same proportionality constant between the reciprocal of compressive yield strength and measured volume per unit energy. The same reasoning that was applied to the shear strength can be applied to the yield strength to indicate why the proportionality K varies. The shear strengths in Table 3 give more consistant results than the compressive yield strengths measured on the Baldwin machine.

Table 4. - Compressive yield strength for the target materials.

Target Material	Yield Strength	(Yield Strength)$^{-1}$	Constant (K)
Lead	0.10×10^{8} newton/m^2	100.00×10^{-9} m^3/joule	23.60
Aluminum	1.02×10^{8}	9.80×10^{-9}	5.87
Magnesium	2.10×10^{8}	4.75×10^{-9}	5.66
Zinc	1.58×10^{8}	6.33×10^{-9}	9.75
Copper	3.35×10^{8}	2.99×10^{-9}	4.99
4140 Steel	7.60×10^{8}	1.31×10^{-9}	6.55

CONCLUSIONS

It has been shown experimentally that the displaced volume of the target is a linear function of the initial energy of the projectile for velocities up to 2.5 kilometers per second. This result is in agreement with the results of Partridge, VanFleet, and Whited.[1, 2] A comparison of the data of this report and their data shows the displaced volume per unit projectile energy is essentially independent of the projectile material. That is, the volume per unit energy is essentially independent if the projectile is RC-66 steel, annealed steel, or of the same material as the target.

It has been further shown experimentally that the plot of crater area versus projectile momentum for the steel projectiles has two linear segments; the momentum at which the segments intersect being the point at which the projectiles were observed to fracture or noticeably deform. The velocity at which the RC-66 steel projectiles fracture was found to be inversely proportional to the target density. This inverse relationship suggests that a hydrodynamic mechanism is causing the pressure on the projectile. A comparison of the results for crater area versus projectile momentum for RC-66 steel projectiles, annealed steel projectiles, and the projectile of the same material as the target indicates that the slope of final segment is independent of the projectile material. The initial linear segment is identical for the two steel projectiles impacted into copper and aluminum. Enough data is not available to determine if this condition for the initial segment exists when the target and projectile are of the same material.

For all the target materials except lead, an essentially constant relationship was found between the reciprocal of the shear strength and the measured crater volume per unit energy. Similarly, a constant relationship was found to exist between the reciprocal of the compressive yield strength and the measured volume per unit energy for all the targets except lead and zinc.

Correlations between penetration data and material properties were not as conclusive as those for volume or area. A region of decrease in penetration for an increase in momentum was found in aluminum, lead, and magnesium. Beyond this region, lead resumed a positive slope for penetration versus momentum, but for the velocity range covered aluminum or magnesium did not show this. Copper, silver, and zinc impacted with RC-66 steel appeared to have two linear regions for penetration versus momentum, while 4140 steel impacted with RC-66 steel and copper impacted with annealed steel appeared to have only one linear region. The point where the penetration started to decrease in aluminum, magnesium, and lead was shown to be the point where the projectile either fractured or started to noticeably deform. Likewise, in copper, silver, and zinc impacted with RC-66 steel, the point where the slope of penetration versus momentum decreased (but remained positive) was also shown to be the point where the projectile fractured.

REFERENCES

1. Partridge, W. S., VanFleet, H. B., Whited, C. R., Technical Report No. OSR-9, AF 18(600)-1217. Part of this report is published under reference 2.

2. Partridge, W. S., VanFleet, H. B., Whited, C. R., "Crater Formation in Metallic Targets," Journal of Applied Physics, 29, 1332-1336 (1958).

3. Lovell, A. C. B., Meteor Astronomy, Oxford University Press, New York, 1954.

4. Van Valkenburg, M. E., Technical Report No. OSR-3, Contract No. AF 18(600)-1217.

5. Rinehart, J. S., "Some Observations on High-Speed Impact," Popular Astronomy, 58, 458 (1950).

6. Van Valkenburg, M. E., Clay, W. G., and Huth, J. H., "Impact Phenomena at High Speed," Journal of Applied Physics, 27, 1123 (1956).

7. Third Symposium on Hypervelocity, I, Armour Research Foundation of Illinois Institute of Technology, Chicago, Illinois, 1959.

8. National Metalizing Corporation, 825 New York Ave., Trenton 8, New Jersey.

9. S K F Industries, Inc., Atlas Ball Division, Philadelphia 32, Pennsylvania.

10. Vennard, J. K., Elementary Fluid Mechanics, John Wiley and Sons, New York, 1956.

11. Bearing Service and Supply Company, 1207 South Main Street, Salt Lake City, Utah.

12. Rinehart, J. S., Pearson, J., Behavior of Metals Under Impulsive Loads, American Society for Metals, Cleveland, Ohio, 1954.

13. American Institute of Physics Handbook, McGraw Hill Book Company, New York, 1957.

14. Eshbach, O. W., Handbook of Engineering Fundamentals, John Wiley and Sons, New York, 1936.

15. O'Rourke, C. E., General Engineering Handbook, McGraw Hill Book Company, New York, 1940.

APPENDIX

Data

Projectile for shots 1 thru 199 was RC-66 steel.

Shot No.	Target	Velocity	Energy	Volume	Area	Momentum	Penetration
		km/sec	joules	cm^3	cm^2	kgm/sec	cm
1	Cu	2.06	939	0.560	1.14	0.909	0.696
2	Cu	1.19	315	0.187	0.51	0.527	0.495
3	Cu	No velocity available					
4	Cu	2.01	887	0.541	1.01	0.884	0.762
5	Cu	2.16	1022	0.588	1.11	0.948	0.716
6	Cu	2.12	987	0.578	1.17	0.932	0.708
7	Cu	No velocity available					
8	Cu	2.13	995	0.565	1.19	0.936	0.691
9	Cu	1.65	596	0.342	0.79	0.724	0.603
10	Cu	1.95	839	0.487	1.00	0.859	0.664
11	Cu	1.70	637	0.368	0.82	0.749	0.625
12	Cu	No velocity available					
13	Cu	No velocity available					
14	Cu	1.10	268	0.143	0.47	0.485	0.492
15	Cu	1.96	848	-	1.03	0.863	0.711
16	Cu	2.21	1075	0.663	1.23	0.973	-
17	Cu	1.87	766	0.485	1.03	0.821	0.668
18	Cu	No velocity available					
19	Cu	0.82	146	0.096	0.26	0.359	0.460
20	Cu	0.99	215	0.153	0.40	0.435	0.449
21	Cu	0.57	71	0.057	0.19	0.250	0.370
22	Cu	0.45	44	0.035	0.17	0.196	0.253
23	Cu	0.42	38	0.028	0.17	0.183	0.217
24	Cu	No velocity available					
25	Cu	1.65	596	0.329	0.75	0.724	0.560
26	Cu	1.27	355	0.182	0.57	0.559	0.490
27	Cu	1.64	592	0.323	0.78	0.722	0.580
28	Cu	0.76	128	0.085	0.23	0.336	0.480
29	Cu	1.36	407	0.222	0.64	0.598	0.500
30	Cu	1.73	655	0.398	0.93	0.759	0.620
31	Cu	1.79	707	0.398	0.93	0.789	0.620
32	Cu	1.73	659	0.376	0.85	0.762	0.610
33	Cu	1.73	655	0.360	0.84	0.759	0.580
34	Cu	2.30	1167	0.690	1.37	1.013	0.750
35	Cu	2.27	1135	0.756	1.33	0.999	0.740
36	Cu	2.27	1135	0.732	1.37	0.999	0.846
37	Cu	No velocity available					

Shot No.	Target	Velocity	Energy	Volume	Area	Momentum	Penetration
		km/sec	joules	cm^3	cm^2	kgm/sec	cm
38	Cu	1.98	859	0.531	1.10	0.869	0.690
39	Cu	2.23	1095	0.697	1.29	0.982	0.731
195	Cu	2.44	1309	0.745	0.70	1.070	0.770
196	Cu	2.50	1375	0.770	1.52	1.100	0.775
40	*Stl	0.52	59	0.016	0.15	0.235	0.122
41	Stl	0.63	87	0.022	0.17	0.274	0.147
42	Stl	0.74	121	0.027	0.19	0.326	0.168
43	Stl	0.97	210	0.040	0.31	0.429	0.191
44	Stl	1.28	363	0.071	0.36	0.565	0.258
45	Stl	1.49	485	0.096	0.41	0.653	0.307
46	Stl	1.62	578	0.116	0.45	0.713	0.339
47	Stl	1.62	578	0.117	0.45	0.713	0.338
48	Stl	1.76	681	0.138	0.51	0.773	0.389
49	Stl	1.80	710	0.150	0.53	0.791	0.425
50	Stl	No velocity available					
51	Stl	1.89	788	0.173	0.57	0.833	0.400
52	Stl	2.10	971	0.188	0.65	0.924	0.481
53	Stl	0.56	68	0.019	0.17	0.245	0.130
54	Stl	0.98	215	0.044	0.31	0.435	0.193
55	Stl	1.32	381	0.075	0.38	0.579	0.277
56	Stl	1.34	393	0.074	0.39	0.588	0.303
57	Stl	1.51	500	0.098	0.42	0.664	0.342
58	Stl	1.60	563	0.112	0.45	0.704	0.356
59	Stl	1.75	676	0.145	0.52	0.771	0.439
60	Stl	2.04	916	0.188	0.66	0.898	0.345
61	Stl	No velocity available					
62	Stl	2.08	955	0.193	0.64	0.917	0.445
63	Stl	1.92	808	0.160	0.57	0.843	0.435
64	Stl	1.68	619	0.128	0.48	0.738	0.405
65	Stl	2.09	962	0.186	0.68	0.920	0.461
66	Stl	2.19	1058	0.209	0.70	0.965	0.493
67	Stl	No velocity available					
68	Stl	2.11	979	0.205	0.69	0.928	0.450
69	Stl	2.19	1058	0.200	0.68	0.965	0.443
70	Stl	2.17	1039	0.205	0.67	0.957	0.447
71	Stl	2.30	1168	0.230	0.71	1.014	0.451
72	Stl	2.20	1067	0.213	0.72	0.969	0.515
73	Stl	No velocity available					
74	Stl	0.44	42	0.010	0.13	0.193	0.116
75	Stl	0.63	88	0.016	0.17	0.278	0.161
76	Stl	1.97	853	0.178	0.59	0.866	0.424
77	Stl	2.02	901	0.183	0.61	0.891	0.423
78	Stl	2.02	894	0.190	0.63	0.887	0.431

*4140 Steel

Shot No.	Target	Velocity	Energy	Volume	Area	Momentum	Penetration
		km/sec	joules	cm^3	cm^2	kgm/sec	cm
79	Stl	1.97	859	0.168	0.61	0.869	0.423
80	Stl	2.02	901	0.190	0.67	0.891	0.406
81	Stl	2.10	971	0.199	0.68	0.924	0.430
82	Stl	2.14	1005	0.200	0.71	0.940	0.435
83	Stl	2.12	996	0.190	0.69	0.936	0.505
84	Pb	Crater ruined					
85	Pb	Crater ruined					
86	Pb	0.63	88	0.598	0.79	0.279	1.440
87	Pb	Crater ruined					
88	Pb	1.28	360	1.770	2.43	0.563	1.076
89	Pb	1.40	434	2.130	2.91	0.618	1.124
90	Pb	1.49	490	2.350	3.09	0.657	1.088
91	Pb	1.51	499	2.330	3.22	0.663	1.160
92	Pb	Crater ruined					
93	Pb	1.83	733	3.163	3.89	0.803	1.293
94	Pb	1.69	628	2.815	3.77	0.743	1.251
95	Pb	1.99	873	3.600	4.50	0.877	1.318
96	Pb	0.44	42	0.300	0.48	0.193	1.030
97	Pb	0.56	69	0.479	0.65	0.246	1.290
98	Pb	0.47	49	0.348	0.52	0.207	1.110
99	Pb	0.97	209	1.065	1.48	0.429	1.230
100	Pb	1.30	368	1.850	2.60	0.570	1.087
101	Pb	2.27	1137	1.880	2.70	1.000	1.135
102	Pb	1.53	514	2.450	3.16	0.673	1.190
103	Pb	1.48	479	2.410	3.19	0.649	1.145
104	Pb	1.66	607	2.700	3.53	0.731	1.259
105	Pb	2.02	901	3.880	4.52	0.891	1.270
106	Pb	Crater ruined					
107	Pb	1.88	777	3.470	4.26	0.827	1.320
108	Pb	Crater ruined					
109	Pb	Crater ruined					
110	Pb	2.17	1040	4.050	4.75	0.956	1.310
111	Pb	Crater ruined					
112	Pb	Crater ruined					
197	Pb	2.38	1247	4.700	5.43	1.050	1.405
198	Pb	2.24	1105	4.400	5.02	0.986	1.345
113	Al	0.12	3	0.009	0.11	0.052	0.093
114	Al	0.57	71	0.180	0.25	0.253	0.670
115	Al	0.66	97	0.183	0.26	0.292	0.830
116	Al	No velocity available					
117	Al	1.03	224	-	0.36	0.444	1.470
118	Al	1.33	391	0.635	0.45	0.587	2.290
119	Al	1.38	417	0.687	0.47	0.606	2.340
120	Al	0.23	12	0.025	0.19	0.103	0.190
121	Al	1.61	569	0.821	0.55	0.707	2.790

Shot No.	Target	Velocity	Energy	Volume	Area	Momentum	Penetration
		km/sec	joules	cm^3	cm^2	kgm/sec	cm
122	Al	1.59	558	0.790	0.50	0.701	2.770
123	Al	1.69	632	0.907	0.54	0.746	2.710
124	Al	1.83	738	1.106	0.66	0.806	2.520
125	Al	No velocity available					
126	Al	1.93	820	1.390	0.82	0.838	2.430
127	Al	2.07	947	1.682	1.00	0.913	1.930
128	Al	Crater ruined					
129	Al	Crater ruined					
130	Al	2.23	1096	2.050	1.17	0.982	1.700
131	Al	0.12	3	0.009	0.11	0.051	0.083
132	Al	0.43	41	0.075	0.22	0.189	0.290
133	Al	1.06	245	0.370	0.30	0.465	1.700
134	Al	1.49	487	0.665	0.43	0.655	2.470
135	Al	2.03	909	1.480	0.87	0.894	2.270
136	Al	2.01	887	1.371	0.82	0.884	2.160
137	Al	Crater ruined					
138	Al	2.28	1147	2.075	1.21	1.005	1.640
000	Al	2.56	1446	2.650	1.54	1.128	1.780
145	Zn	0.37	30	0.019	0.07	0.161	0.201
146	Zn	0.57	72	0.056	0.19	0.251	0.350
147	Zn	0.74	120	0.083	0.22	0.325	0.440
148	Zn	0.91	183	0.137	0.27	0.402	0.570
149	Zn	1.26	351	0.220	0.52	0.556	0.532
150	Zn	1.46	470	0.304	0.64	0.643	0.600
151	Zn	1.63	587	0.420	0.84	0.710	0.660
152	Zn	1.61	569	0.371	0.72	0.708	0.680
153	Zn	1.70	632	0.383	0.72	0.746	0.653
154	Zn	1.75	677	0.410	0.79	0.772	0.675
155	Zn	1.74	663	0.410	0.77	0.764	0.691
156	Zn	1.90	802	0.513	0.95	0.836	0.761
157	Zn	2.03	909	0.575	1.04	0.895	0.728
158	Zn	2.51	1389	0.890	1.54	1.110	0.783
159	Zn	0.45	45	0.035	0.18	0.199	0.265
160	Zn	0.72	115	0.085	0.23	0.318	0.443
161	Zn	1.26	351	0.270	0.41	0.556	0.575
162	Zn	1.58	548	0.595	0.72	0.694	0.654
163	Zn	1.57	611	0.490	0.76	0.738	0.667
164	Zn	1.65	595	0.400	0.69	0.725	0.643
165	Zn	1.89	783	0.510	0.92	0.830	0.713
166	Ag	No velocity available					
167	Ag	No velocity available					
168	Ag	0.65	94	0.120	0.23	0.285	0.600
169	Ag	0.50	55	0.068	0.20	0.220	0.440
170	Ag	0.70	107	0.112	0.25	0.307	0.610
171	Ag	0.64	90	0.095	0.24	0.281	0.540

Shot No.	Target	Velocity	Energy	Volume	Area	Momentum	Penetration
		km/sec	joules	cm^3	cm^2	kgm/sec	cm
172	Ag	1.25	344	0.300	0.72	0.550	0.644
173	Ag	1.22	327	0.295	0.75	0.537	0.639
174	Ag	1.02	229	0.215	0.52	0.449	0.594
175	Ag	1.67	611	0.530	1.06	0.733	0.724
176	Ag	1.85	749	0.650	1.19	0.812	0.764
177	Ag	1.73	659	0.620	1.21	0.761	0.763
178	Ag	1.87	772	0.720	1.32	0.824	0.739
179	Ag	1.78	696	0.650	1.27	0.783	0.761
180	Ag	2.54	1417	1.240	2.03	1.117	0.924
181	Ag	0.79	199	0.170	0.29	0.349	0.640
182	Ag	1.00	220	0.225	0.41	0.440	0.658
183	Mg	0.63	88	0.082	0.17	0.279	0.550
184	Mg	No velocity available					
185	Mg	0.85	158	0.137	0.19	0.373	0.880
186	Mg	0.98	213	0.182	0.18	0.433	1.150
187	Mg	1.11	272	0.227	0.20	0.489	1.400
188	Mg	1.52	505	0.407	0.25	0.667	2.290
189	Mg	1.39	424	0.337	0.23	0.611	1.960
190	Mg	1.62	580	0.432	0.26	0.714	2.430
191	Mg	1.89	785	0.597	0.32	0.831	3.010
192	Mg	1.96	846	0.667	0.33	0.863	3.230
193	Mg	2.27	1137	0.717	0.37	1.000	3.300
194	Mg	2.38	1247	1.100	0.50	1.047	3.020
199	Mg	0.39	35	-	0.15	0.173	0.150
Projectile for shots 200 thru 223 was annealed steel.							
200	Al	0.55	66	0.110	0.20	0.241	0.610
201	Al	0.83	153	0.210	0.26	0.367	1.000
202	Al	No velocity available					
203	Al	0.86	163	0.240	0.28	0.378	1.210
204	Al	1.35	401	0.520	0.45	0.594	1.620
205	Al	1.23	334	0.630	0.55	0.540	1.780
206	Al	1.44	456	0.650	0.53	0.633	1.820
207	Al	1.55	528	0.730	0.64	0.682	1.800
208	Al	1.95	836	1.220	1.04	0.858	1.680
209	Al	1.94	828	1.200	1.06	0.854	1.660
210	Al	2.15	1017	1.460	1.25	0.946	1.660
211	Al	2.18	1045	1.550	1.31	0.959	1.620
212	Al	2.33	1195	1.720	1.47	1.025	1.840
213	Cu	0.47	50	0.330	0.20	0.207	0.244
214	Cu	No velocity available					
215	Cu	1.05	243	0.140	0.49	0.462	0.430
216	Cu	0.95	199	0.120	0.43	0.419	0.387
217	Cu	1.49	48	0.240	0.62	0.656	0.528

Shot No.	Target	Velocity	Energy	Volume	Area	Momentum	Penetration
		km/sec	joules	cm^3	cm^2	kgm/sec	cm
218	Cu	1.58	620	0.310	0.81	0.695	0.619
219	Cu	1.85	753	0.430	0.85	0.814	0.588
220	Cu	1.62	577	0.330	0.81	0.713	0.613
221	Cu	1.97	854	0.440	1.02	0.867	0.652
222	Cu	1.36	420	0.240	0.66	0.608	0.527
223	Cu	2.09	961	0.510	1.11	0.920	0.672